Adaptive vibration-based bearing fault diagnosis for mud pumps using MSESSA-optimized variational mode decomposition

Chao Zhang[1], Bing Wang[2], Zhenzhong Zhang[3]
[1, 2]CNOOC (China) Limited Tianjin Branch, Tianjin, China
[3]Changzhou University, Changzhou, China
[3]Corresponding author
E-mail: [1]*Zhangchao7@cnooc.com.cn*, [2]*wangbing4@cnooc.com.cn*, [3]*zzz6399@163.com*

Received 13 January 2026; accepted 18 March 2026; published online 8 May 2026
DOI https://doi.org/10.21595/jve.2026.26008

Abstract. Mud pumps operate under harsh conditions, where strong background noise, load fluctuations, and complex excitations result in highly non-stationary vibration signals, posing significant challenges for reliable bearing fault diagnosis. To address these challenges, this study proposes an adaptive vibration-based fault diagnosis framework for mud pump bearings, utilizing variational mode decomposition optimized by a multi-strategy enhanced sparrow search algorithm (MSESSA-VMD). The proposed MSESSA incorporates sine–cosine perturbation, Cauchy mutation, and adaptive weight updating mechanisms to enhance global exploration and convergence stability. In contrast to conventional SSA-based optimization approaches, this strategy enables automatic and robust optimization of key VMD parameters, including the number of decomposition modes and the penalty factor, thereby improving decomposition quality under complex operating conditions. Fault-relevant intrinsic mode functions (IMFs) are subsequently selected based on energy-based criteria for multi-dimensional feature extraction. Intelligent fault classification is then performed using a Light Gradient Boosting Machine (LightGBM) classifier. The effectiveness of the proposed framework is first verified using the benchmark Case Western Reserve University (CWRU) bearing dataset and further validated on simulated mud pump bearing vibration signals to assess robustness under industrial-like operating conditions. Experimental results demonstrate that the proposed method achieves an average diagnostic accuracy of 96.14 %, outperforming conventional VMD-based and SSA-VMD approaches in terms of accuracy and robustness against noise and signal non-stationarity. Overall, this study presents a novel framework that integrates a multi-strategy enhanced sparrow search mechanism with adaptive VMD parameter optimization for mud pump bearing fault diagnosis, providing a robust and generalizable solution for vibration-based machinery health monitoring in complex industrial environments.

Keywords: variational mode decomposition, sparrow search algorithm, adaptive optimization, bearing fault diagnosis, mud pump vibration, machine learning.

1. Introduction

Mud pumps are critical components in drilling systems, and their operating conditions directly affect drilling efficiency, equipment reliability, and operational safety. During long-term operation under harsh environments, key rotating components such as bearings are subjected to heavy loads, complex mechanical excitations, and severe environmental disturbances. These factors generate highly nonlinear and non-stationary vibration responses, significantly increasing the difficulty of fault detection and condition monitoring [1-4].

In practical industrial settings, vibration signals collected by sensors are often contaminated by strong background noise and external disturbances, rendering fault-related features weak and difficult to extract. Failure to detect bearing faults in a timely manner may lead to unexpected equipment failures, drilling interruptions, or even serious safety accidents [5-7]. Consequently,

developing reliable vibration signal processing techniques and intelligent fault diagnosis methods for rotating machinery has become a critical research topic in condition monitoring and predictive maintenance [8-10]. In particular, data-driven fault diagnosis approaches based on feature selection and data mining techniques have demonstrated promising performance in complex industrial systems [11].

Signal decomposition techniques have recently gained significant attention for analyzing nonlinear and non-stationary vibration signals. Among them, Empirical Mode Decomposition (EMD) is widely used due to its adaptive nature and ability to decompose complex signals into intrinsic mode functions (IMFs) without requiring predefined basis functions [12]. EMD has been applied extensively in the fault diagnosis of rotating machinery, including bearings, pumps, and gearboxes [13-15]. However, classical EMD suffers from intrinsic limitations such as mode mixing, end effects, and sensitivity to noise, which can compromise the reliability of extracted features [16]. To mitigate these issues, variants such as Ensemble Empirical Mode Decomposition (EEMD) and complementary ensemble methods have been proposed [17, 18]. Although these methods can partially alleviate mode mixing, they may introduce reconstruction errors and increase computational complexity.

Variational Mode Decomposition (VMD) has emerged as a robust alternative to EMD, formulating signal decomposition as a constrained variational optimization problem to extract a predefined number of band-limited IMFs. Compared with traditional EMD, VMD offers improved noise robustness, reduced mode mixing, and enhanced decomposition stability [19-22], and it has been widely employed in vibration analysis, fault feature extraction, and condition monitoring of rotating machinery [24-25]. The effectiveness of VMD critically depends on selecting key parameters, particularly the number of decomposition modes K and the penalty factor \alpha. Improper settings may lead to under- or over-decomposition, reducing feature quality and diagnostic accuracy [26].

To address this, intelligent optimization algorithms have been employed to automatically determine optimal VMD parameters. Genetic algorithms and other evolutionary methods have been widely applied to fault diagnosis as well as broader engineering optimization problems [27, 28]. Swarm intelligence algorithms, including particle swarm optimization (PSO), artificial fish swarm algorithm, and gray wolf optimizer, are also commonly adopted for this purpose [29-31]. More recently, the Sparrow Search Algorithm (SSA), inspired by the foraging and anti-predation behaviors of sparrows, has shown promising performance in complex optimization tasks due to its simple structure, fast convergence, and strong global search capability [32-35]. However, conventional SSA may still suffer from insufficient population diversity and a tendency to become trapped in local optima during later iterations.

To overcome these limitations, numerous SSA variants have been proposed by incorporating mechanisms such as chaotic mapping, adaptive weight updating, sine-cosine perturbations, and mutation operators [36-38]. These strategies aim to balance global exploration and local exploitation, improving convergence stability and optimization accuracy in complex search spaces.

After signal decomposition, selecting the most informative IMFs that contain significant fault information is another critical step in the fault diagnosis process. Directly using all decomposed modes may introduce redundant or noise-dominated components, which can increase feature dimensionality and negatively affect classification performance [39]. Therefore, effective IMF evaluation and selection strategies are essential for improving feature quality and diagnostic reliability.

Energy-based indicators and statistical impulsiveness measures have been widely used to identify fault-sensitive signal components [40]. Among them, the Energy Contribution Ratio (ECR) reflects the relative energy distribution of each IMF, while the Peak Factor (PF) is highly sensitive to impulsive fault signatures, making them effective indicators for early-stage bearing fault detection [41].

In addition to signal processing and feature extraction techniques, the performance of a fault

diagnosis system is also strongly influenced by the effectiveness of the classification algorithm. Traditional machine learning methods, such as support vector machines and k-nearest neighbor classifiers, have been widely used in rotating machinery fault diagnosis. However, their performance may deteriorate when handling high-dimensional nonlinear features or large-scale datasets. Recently, ensemble learning models have demonstrated strong performance in industrial diagnosis tasks due to their ability to integrate multiple weak learners and improve prediction robustness.

Among these methods, Light Gradient Boosting Machine (LightGBM) has attracted increasing attention because of its efficient histogram-based feature discretization and leaf-wise tree growth strategy, which significantly improve computational efficiency while maintaining high classification accuracy. Furthermore, integrating automated hyperparameter optimization techniques can further enhance model stability and reduce dependence on empirical parameter tuning.

Motivated by the above challenges, this study proposes an adaptive vibration-based fault diagnosis framework for mud pump bearings by integrating a multi-strategy enhanced sparrow search algorithm (MSESSA), optimized VMD decomposition, and LightGBM classification. In the proposed framework, MSESSA is first employed to automatically determine the optimal parameters of VMD, thereby improving the decomposition quality of nonlinear and non-stationary vibration signals.

Subsequently, an IMF selection strategy based on the combined Energy Contribution Ratio and Peak Factor is introduced to identify fault-relevant signal components while suppressing noise-dominated modes. Finally, statistical features extracted from the selected IMFs are used to train a LightGBM classifier for accurate fault identification.

The effectiveness of the proposed method is validated using the widely used Case Western Reserve University (CWRU) bearing dataset and further evaluated using simulated mud pump vibration signals under representative operating conditions, including load variations, noise interference, and non-stationary excitations. Experimental results demonstrate that the proposed framework outperforms conventional VMD-based and SSA-VMD approaches in terms of diagnostic accuracy and robustness against noise and signal non-stationarity.

Compared with existing VMD-based or SSA-based diagnostic approaches, the proposed framework provides several improvements. First, unlike conventional SSA-VMD methods that rely on single enhancement strategies or static parameter control, the proposed multi-strategy enhanced sparrow search algorithm (MSESSA) integrates complementary mechanisms to improve both global exploration and local exploitation, resulting in more stable convergence and more reliable optimization performance.

Second, while most existing studies focus primarily on VMD parameter optimization, this study introduces a joint IMF selection strategy based on the Energy Contribution Ratio (ECR) and Peak Factor (PF), which effectively refines decomposition results and suppresses noise-dominated components.

Third, instead of adopting computationally intensive deep learning architectures, a lightweight Light Gradient Boosting Machine (LightGBM) classifier is employed, achieving efficient training, strong generalization ability, and improved practicality for engineering applications. By integrating these components, an adaptive and robust fault diagnosis framework for mud pump bearings is established.

The remainder of this paper is organized as follows. Section 2 introduces the proposed MSESSA-VMD-LightGBM model and the corresponding optimization strategy. Section 3 presents the overall fault diagnosis framework. Section 4 provides experimental validation and comparative analysis using the CWRU bearing dataset. Section 5 further evaluates the applicability of the proposed method using simulated mud pump vibration signals under representative operating conditions. Finally, Section 6 summarizes the main conclusions and discusses future research directions.

The main contributions and innovations of this study can be summarized as follows. Unlike

conventional SSA–VMD approaches that typically rely on a single enhancement strategy or static parameter control, the proposed framework integrates multiple improvement mechanisms to achieve more stable parameter optimization and improved diagnostic performance under complex operating conditions.

(1) A novel multi-strategy enhanced sparrow search algorithm (MSESSA) is proposed by incorporating sine–cosine perturbation, Cauchy mutation, and adaptive weight updating mechanisms. These strategies effectively enhance the global exploration capability and convergence stability of the conventional SSA in complex optimization spaces.

(2) An adaptive VMD parameter optimization framework is developed to automatically determine the optimal number of decomposition modes and the penalty factor. This approach reduces reliance on empirical parameter selection and improves the robustness of signal decomposition for highly nonlinear and non-stationary vibration signals.

(3) A comprehensive vibration-based fault diagnosis framework for mud pump bearings is established by integrating optimized VMD decomposition, fault-relevant IMF selection based on Energy Contribution Ratio and Peak Factor, multidimensional feature extraction, and LightGBM-based classification into a unified end-to-end diagnostic process.

(4) Extensive experiments conducted on both the CWRU benchmark dataset and simulated mud pump vibration signals demonstrate that the proposed framework achieves higher diagnostic accuracy and stronger robustness against noise interference and signal non-stationarity compared with conventional VMD-based and SSA-VMD diagnostic approaches, highlighting its potential applicability in intelligent condition monitoring of industrial mud pump systems.

2. Fault diagnosis model based on MSESSA-VMD-LightGBM

2.1. MSESSA-VMD

In fault diagnosis, variational mode decomposition (VMD) has been widely adopted to extract intrinsic modal components from vibration signals. The decomposition performance of VMD is highly dependent on parameter selection, particularly the number of modes K and the penalty factor α, which jointly determine the bandwidth and resolution of each mode. Inappropriate parameter settings may lead to mode mixing, over-decomposition, or loss of fault-related information.

In most existing studies, VMD parameters are determined empirically or through exhaustive search, which is time-consuming and lacks adaptability to varying operating conditions. To address this issue, this study introduces a multi-strategy enhanced sparrow search algorithm (MSESSA) for automatic optimization of VMD parameters, aiming to improve the adaptability, stability, and decomposition performance of VMD in fault diagnosis applications.

The core idea of VMD is to assume that the original signal $f(t)$ consists of several sub-signals $\{u_k(t)\}_{k-1}^{K}$ with finite bandwidths, each corresponding to a distinct center frequency ω_k. The objective of VMD is to make each mode as compact as possible in the frequency domain – that is, to minimize the sum of their bandwidths – thereby achieving an adaptive decomposition of the signal. Specifically, the variational model of VMD can be expressed as:

$$\min_{\{u_k\},\{\omega_k\}} \left\{ \sum_{k=1}^{K} \left\| \partial_t \left[\left(\delta(t) + \frac{j}{\pi t} \right) * u_k(t) \right] e^{-j\omega_k t} \right\| 2^2 \right\}, \tag{1}$$

where, * denotes the convolution operation, ∂_t represents the partial derivative with respect to time, and $\delta(t)$ is the impulse response function. The physical significance of this optimization problem lies in constraining the bandwidth of each mode in the frequency domain, thereby assigning distinct center frequencies to different modes and achieving adaptive signal decomposition.

To solve this optimization problem, VMD introduces the Lagrange multiplier $\lambda(t)$ and the penalty factor α to construct an augmented Lagrange function:

$$L(\{u_k\},\{\omega_k\},\lambda) = \alpha \sum_{k=1}^{K} \left\| \partial_t \left[\left(\delta(t) + \frac{j}{\pi t} \right) * u_k(t) \right] e^{-j\omega_k t} \right\| 2^2 + \left\| f(t) - \sum k = 1^K u_k(t) \right\| 2^2 + \left\langle \lambda(t), f(t) - \sum k = 1^K u_k(t) \right\rangle. \quad (2)$$

Using the Alternating Direction Method of Multipliers (ADMM), VMD alternately updates each mode u_k, center frequency ω_k, and Lagrange multiplier $\lambda(t)$ until convergence criteria are met. The iterative update steps can be summarized as follows:

(1) Update each modal component u_k: Update its spectral representation in the frequency domain to minimize bandwidth at the given center frequency.

(2) Update center frequency ω_k: Calculate the energy center of the current modal spectrum to dynamically adjust the center frequency.

(3) Update Lagrange multiplier $\lambda(t)$: Ensure the reconstructed signal of each mode matches the original signal.

SSA classifies individuals within a population into three categories: Discoverers, Joiners, and Scouts. Discoverers perform global search and directional guidance, possessing higher energy to explore broader spaces; Joiners conduct local search and follow position updates based on Discoverers to enhance convergence; Scouts monitor potential threats in the environment (such as getting stuck in local optima) and help the population escape local optima traps through mutation or jump strategies.

Their position update models are as follows:

– Discoverer position update:

$$X_i^{t+1} = X_i^t \cdot e^{-\frac{i}{\alpha \cdot T}}, \quad (3)$$

$$X_i^{t+1} = X_i^t + Q \cdot L, \quad (4)$$

where Q is a random number following a normal distribution, L is the random stride, and α is the control parameter.

– Participant position update:

$$X_i^{t+1} = Q \cdot e^{\frac{X_{worst}^t - X_i^t}{(X_{best}^t - X_i^t + e)}}. \quad (5)$$

Among them, X_{best}^t and X_{worst}^t represent the current global best and worst individuals, respectively.

– Sentinel position update:

$$X_i^{t+1} = X_{best}^t + \beta \cdot |X_i^t - X_{best}^t|, \quad (6)$$

where, β represents a disturbance factor following a standard normal distribution, used to simulate the random jumping behavior of sparrows when threatened.

In the conventional Sparrow Search Algorithm (SSA), position updates are governed by predefined behavioral rules, which may limit adaptability during complex optimization tasks. Although SSA is designed to balance global exploration and local exploitation, its performance may degrade when solving high-dimensional or multimodal problems. In particular, insufficient population diversity in the early search stages can restrict exploration coverage, while limited refinement capability in later iterations may result in premature convergence to local optima.

To address these limitations, this study proposes a Multi-Strategy Enhanced Sparrow Search

Algorithm (MSESSA). The proposed approach incorporates three complementary enhancement mechanisms to improve population diversity, strengthen local exploitation accuracy, and enhance overall convergence stability.

(1) Sine-cosine mechanism.

During the early exploration phase, the standard SSA initialization and position update strategy may lead to uneven population distribution and inadequate global search coverage. To mitigate this issue, a sine-cosine perturbation mechanism is embedded into the position update process. By introducing oscillatory adjustments based on sine and cosine functions, individual positions are adaptively perturbed with dynamic step sizes. This periodic search behavior enlarges the exploration range and increases population diversity during early iterations, thereby improving the algorithm's ability to escape poor initial regions and explore the solution space more effectively. The corresponding position update formula is defined as follows:

$$X_i^{t+1} = X_i^t + r_1 \times \sin(r_2) \times |r_3 \times X_{best}^t - X_i^t|. \tag{7}$$

Among these, r_1, r_2 and r_3 are random factors used to control the search amplitude and direction. This mechanism implicitly introduces a periodic global perturbation behavior, which shares a similar exploratory effect with random walk-based strategies.

(2) Cauchy mutation strategy.

In the middle and later stages of the optimization process, the population in standard SSA may gradually lose diversity, increasing the risk of premature convergence to local optima. To enhance the algorithm's ability to escape such stagnation, a Cauchy mutation operator is applied to selected elite individuals. Due to its heavy-tailed probability distribution, the Cauchy function occasionally generates large perturbations, enabling long-distance transitions in search space. These sporadic large-step updates help the algorithm escape local minimum while preserving exploitation around promising regions. Consequently, population diversity is maintained, and the global search robustness of the algorithm is improved. The mutation process can be expressed as follows:

$$X_{new} = X_{elite} + \delta \times C(0,1), \tag{8}$$

where, $C(0,1)$ denotes a random variable following a standard Cauchy distribution, where δ is the coefficient of variation. Compared with Gaussian mutation, the heavy-tailed distribution of the Cauchy operator provides stronger long-distance exploration capability.

(3) Adaptive weighting mechanism.

To achieve a dynamic balance between exploration and exploitation during the entire optimization process, an adaptive weighting mechanism is introduced. The adaptive weight is designed to vary with the iteration number: larger weights are assigned in early iterations to encourage broader exploration, while gradually decreasing weights in later iterations promote refined local search. This progressive adjustment allows the algorithm to transition smoothly from coarse global search to fine-grained exploitation. As a result, convergence efficiency is enhanced and solution accuracy is improved in the later optimization stages. The adaptive weighting scheme is defined as:

$$\omega = \omega \left(\omega min_{max} \times \frac{t}{T_{max}} \right)_{max}. \tag{9}$$

As iterations progress, the adaptive weights in MSESSA gradually decrease, allowing the algorithm to shift smoothly from broad global exploration to fine-grained local exploitation. This adjustment enhances convergence efficiency and search precision, reduces the need for manual parameter tuning, and improves robustness under varying signal conditions. The multi-strategy enhancements – including sine-cosine perturbation, Cauchy mutation, and adaptive weight updating – strengthen global exploration, prevent premature convergence, and maintain

population diversity. Sine-cosine perturbation guides sparrows toward unexplored regions, while Cauchy mutation introduces stochastic variation to elite individuals, helping escape local optima.

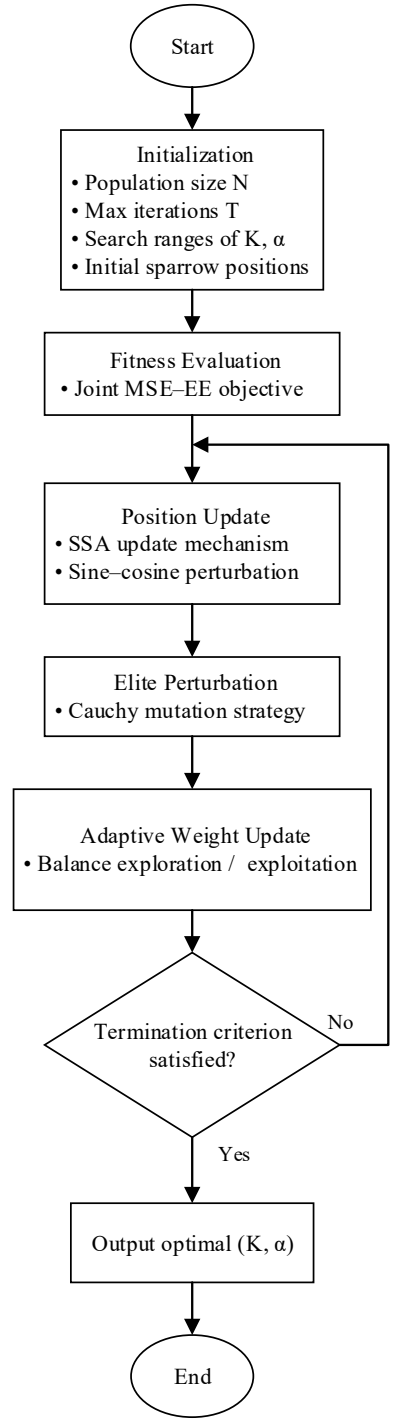

Fig. 1. Flowchart of the proposed multi-strategy enhanced sparrow search algorithm (MSESSA) for VMD parameter optimization

The overall procedure of MSESSA is illustrated in Fig. 1. The population size, maximum iterations, and search ranges for key VMD parameters are initialized, and the initial sparrow population is generated randomly. The fitness of each individual is evaluated using the joint MSE-EE objective function, balancing reconstruction fidelity and fault information concentration. During each iteration, sparrow positions are updated according to standard SSA rules, enhanced by the sine-cosine perturbation, and elite individuals undergo Cauchy mutation. Adaptive weights are adjusted dynamically, gradually shifting the emphasis from exploration to exploitation.

Compared with conventional SSA, MSESSA demonstrates improved convergence stability and global search capability, ensuring that optimal VMD parameters are selected. This results in intrinsic mode functions with high modal independence and concentrated fault-related energy, providing a reliable basis for subsequent feature extraction and fault classification.

The detailed optimization procedure of the proposed MSESSA-VMD framework is summarized in Table 1.

Table 1. MSESSA-VMD parameter optimization framework

Input:
Raw vibration signal $x(t)$
Population size N
Maximum iteration T_{max}
Search ranges of K and α

Output:
Optimal parameters K^*, α^*
Optimal decomposed IMFs

Initialize sparrow population $X_i = [K_i, \alpha_i]$, $i = 1, 2,...,N$
Randomly generate K_i and α_i within predefined bounds
For each X_i:
    Perform VMD decomposition using (K_i, α_i)
    Compute fitness = MSE + Energy Entropy (EE)
End For

$t = 1$
While ($t \leq T_{max}$) do
    Rank population according to fitness
    Identify discoverers and joiners

    Update discoverers using sine-cosine perturbation
    Apply Cauchy mutation to selected individuals
    Update adaptive weight parameters

    Apply boundary control to K_i and α_i
    Round Ki to nearest integer

    For each updated X_i:
        Perform VMD decomposition
        Recalculate fitness
    End For

    Update global best solution (K^*, α^*)
    $t = t + 1$
End While

Perform final VMD using (K^*, α^*)
Return optimal parameters and IMFs

Table 1 illustrates the iterative optimization procedure, in which VMD parameters are adaptively updated through sine–cosine perturbation, Cauchy mutation, and adaptive weighting mechanisms.

To guide the adaptive optimization of VMD parameters, a composite fitness function integrating Mean Squared Error (MSE) and Envelope Entropy (EE) is employed as the primary evaluation criterion of the proposed MSESSA framework.

The MSE quantifies the reconstruction accuracy between the original vibration signal and the signal reconstructed by VMD, reflecting the fidelity of signal approximation. Lower MSE values indicate higher reconstruction accuracy and reduced signal distortion during decomposition.

The EE characterizes the energy distribution of the signal envelope and captures the concentration and independence of energy among the decomposed intrinsic mode functions (IMFs). Smaller EE values correspond to more concentrated modal energy and reduced inter-component coupling, thereby enhancing the sensitivity to fault-related features.

Relying on a single evaluation index may yield suboptimal decomposition. Minimizing MSE alone can achieve accurate signal reconstruction but may result in mode overlaps, whereas focusing solely on EE may improve modal separation at the expense of reconstruction fidelity. To overcome these limitations, MSE and EE are jointly incorporated into a unified fitness function, enabling a balanced assessment of reconstruction accuracy and modal independence. The optimization objective is defined as:

$$F = \omega_1 \cdot MSE + \omega_2 \cdot EE, \tag{10}$$

where ω_1 and ω_2 denote the weighting coefficients used to balance the contributions of MSE and EE during the optimization process.

By simultaneously accounting for signal reconstruction fidelity and fault-sensitive energy distribution, the proposed joint fitness function effectively improves the independence and discriminability of the decomposed modal components while ensuring stable and accurate VMD decomposition. When combined with the multi-strategy enhancements embedded in MSESSA, this fitness-driven optimization process achieves a favorable balance between global exploration and local exploitation, leading to improved convergence stability and robustness.

As a result, the proposed MSESSA-VMD framework provides a reliable and physically meaningful basis for adaptive parameter optimization, high-quality signal decomposition, and intelligent bearing fault diagnosis, specifically tailored to mud pump applications.

2.2. IMF decomposition and feature extraction

After completing the MSESSA-optimized VMD decomposition, the original vibration signal is adaptively separated into a series of intrinsic mode functions (IMFs), each capturing distinct frequency components and oscillatory behaviors. However, not all IMFs contribute equally to fault diagnosis, as some may be dominated by noise or irrelevant background vibrations. Therefore, an effective selection strategy is essential to retain fault-relevant modes while suppressing redundant components.

In this study, IMF selection is performed using a combined evaluation of the Energy Contribution Ratio (ECR) and the Peak Factor (PF). The ECR measures the proportion of total signal energy contributed by each IMF and is defined as the ratio between the energy of an individual IMF and the total energy of all IMFs. IMFs with higher ECR values generally capture the dominant vibration energy of the system and reflect its primary dynamic characteristics:

$$ECR_i = \frac{\sum_{t=1}^{N}\left(IMF_i(t)\right)^2}{\sum_{j=1}^{K}\sum_{t=1}^{N}\left(IMF_j(t)\right)^2}. \tag{11}$$

IMFs with high energy contribution ratios typically contain the primary vibration of energy information of the equipment.

The PF, defined as the ratio of the maximum absolute amplitude to the root mean square value, is widely used for detecting impulsive and transient components in vibration signals. It is particularly sensitive to localized defects and early-stage bearing faults, which often generate high-amplitude impact responses. Consequently, IMFs with larger PF values are more likely to contain fault-related impulsive features:

$$PF_i = \frac{max(|IMF_i(t)|)}{\sqrt{\frac{1}{N}\sum_{t=1}^{N}\left(IMF_i(t)\right)^2}}. \tag{12}$$

IMFs with higher peak factors often correspond to fault impact responses in bearings or mechanical components.

To ensure that selected IMFs exhibit both significant energy contribution and strong fault sensitivity, a weighted composite criterion is adopted:

$$S_i = \lambda_1 \cdot ECR_i + \lambda_2 \cdot PF_i, \tag{13}$$

where ECR_i and PF_i denote the energy contribution ratio and peak factor of the i-th IMF, respectively, and λ_1 and λ_2 are weighting coefficients. In this work, both weights are set to 0.5 to balance energy dominance and impulsive fault characteristics. The IMFs with the highest composite scores are selected for subsequent analysis.

By jointly considering the ECR and PF metrics, the proposed IMF selection strategy effectively retains modal components that contain dominant fault-related information while suppressing noise-dominated or low-informative modes. This approach enhances both the fidelity and robustness of signal reconstruction.

Based on the selected IMFs, a set of multidimensional features is extracted to comprehensively characterize the equipment's operational state. These features encompass time-domain statistical indicators, including mean, variance, skewness, and kurtosis, as well as frequency-domain descriptors that capture energy distribution characteristics, such as maximum frequency, spectral bandwidth, and center frequency.

This comprehensive feature set captures both the dynamic and spectral properties of the vibration signals, providing discriminative and reliable inputs for subsequent fault diagnosis and classification models.

2.3. Fault diagnosis based on LightGBM

After performing signal decomposition using the proposed MSESSA-VMD framework and conducting IMF selection and feature extraction, a Light Gradient Boosting Machine (LightGBM) classifier is employed for bearing fault diagnosis. LightGBM is an efficient gradient boosting framework based on decision tree ensembles, particularly suitable for handling high-dimensional feature sets with complex nonlinear relationships. By leveraging histogram-based feature discretization and a leaf-wise tree growth strategy, LightGBM achieves an effective balance between computational efficiency and classification accuracy.

In this study, the classifier is trained to identify four bearing operating conditions: normal state, inner race fault, outer race fault, and rolling element fault, based on the extracted vibration features.

(1) Model principle.

LightGBM constructs an ensemble of decision trees iteratively through boosting. At each iteration, a new tree is trained to fit the negative gradient (residual) of the loss function relative to the current model output, thereby progressively minimizing the overall objective function. Unlike

level-wise tree growth strategies, LightGBM employs a leaf-wise growth mechanism that prioritizes splitting leaf nodes with the largest information gain. This approach enables faster convergence and improved learning capability for complex decision boundaries. The general optimization objective can be expressed as:

$$L = \sum_{i=1}^{n} l\left(y_i, \hat{y}_i^{(t-1)} + f_t(x_i)\right) + \Omega\left(f_t\right), \tag{14}$$

where, $l(\cdot)$ denotes the loss function, $f_t(x_i)$ represents the predicted output of the t-th tree, and $\Omega(f_t)$ signifies the regularization term for model complexity. LightGBM employs gradient-based one-sided sampling (GOSS) and exclusive feature bundling (EFB) strategies, significantly accelerating training speed while maintaining model accuracy.

(2) Feature input and model training.

Based on the MSESSA-VMD decomposition and the proposed ECR-PF-based IMF selection, a multidimensional feature vector is constructed from the selected IMFs. The feature set includes time-domain statistical indicators (e.g., mean, variance, skewness, kurtosis) and frequency-domain descriptors that reflect energy distribution characteristics. Together, these features capture both the dynamic behavior and spectral properties of the bearing vibration signals under different operating conditions.

The extracted features are input into the LightGBM classifier for fault identification. During training, LightGBM automatically learns discriminative feature-splitting rules through gradient-based optimization and leaf-wise growth. To evaluate generalization performance and mitigate overfitting, five-fold cross-validation (5-fold CV) is applied. Diagnostic performance is quantitatively assessed using Accuracy (ACC), Precision (PREC), Recall (REC), and F1 score.

Compared with conventional machine learning methods, LightGBM demonstrates superior training efficiency and scalability for high-dimensional feature spaces. Additionally, its tree-based structure allows feature importance analysis, providing insight into the contribution of individual statistical and spectral features to fault classification. When integrated with the optimized MSESSA-VMD-based feature extraction framework, LightGBM achieves robust and reliable fault diagnosis for bearing systems, illustrating its strong applicability for mud pump condition monitoring under complex, non-stationary operating conditions.

3. Fault diagnosis process based on MSESSA-VMD and LightGBM

This study proposes a rolling bearing fault diagnosis framework that integrates MSESSA-optimized Variational Mode Decomposition (MSESSA-VMD) with a Light Gradient Boosting Machine (LightGBM) classifier. The framework aims to effectively extract fault-sensitive features from complex vibration signals and achieve accurate identification of bearing fault conditions. The overall workflow of the proposed approach is summarized as follows:

(1) Data acquisition:

Vibration signals are collected from rolling bearing systems operating under different conditions, including normal operation and typical fault states such as inner race defects, outer race defects, and rolling element faults. These signals are measured using vibration sensors mounted on the bearing housing and are recorded under controlled experimental conditions. The collected signals serve as the primary input to the proposed diagnostic framework.

(2) Signal preprocessing and decomposition:

The raw vibration signals are first preprocessed through normalization and noise suppression to reduce the influence of environmental disturbances and amplitude fluctuations. Subsequently, the MSESSA-VMD algorithm is employed to adaptively decompose each signal into multiple intrinsic mode functions (IMFs) with distinct frequency characteristics. Through automatic optimization of the decomposition parameters, the proposed method ensures that the obtained

IMFs provide a high-fidelity representation of the underlying vibration dynamics while minimizing mode mixing and information loss.

(3) Component selection:

To identify fault-relevant IMFs while suppressing noise-dominated or redundant components, the energy contribution ratio (ECR) and peak factor (PF) of each IMF are calculated as joint evaluation criteria. The ECR reflects the relative energy distribution of each mode, while the PF is sensitive to impulsive characteristics associated with bearing faults. IMFs exhibiting relatively high ECR and PF values are therefore retained for subsequent analysis.

(4) Feature extraction:

Multidimensional statistical features are extracted from the selected IMFs to characterize the vibration behavior of the bearing system. These features include time-domain descriptors such as mean value, variance, skewness, and kurtosis, as well as frequency-domain characteristics including spectral energy distribution, bandwidth, and center frequency. The combination of these complementary features provides a comprehensive representation of the bearing operating condition.

(5) Model training and optimization:

The extracted feature vectors are used as inputs to train the LightGBM classifier. During the training process, gradient boosting learning and cross-validation strategies are employed to optimize the model parameters and prevent overfitting. This process enables the classifier to effectively capture the nonlinear relationships between extracted features and corresponding fault categories.

(6) Fault identification and evaluation:

For the diagnostic stage, unseen vibration signals are processed following the same procedure and then fed into the trained LightGBM model for intelligent identification of bearing fault types. The diagnostic performance of the proposed framework is quantitatively evaluated using multiple classification metrics, including accuracy, precision, recall, and F1-score, ensuring a comprehensive assessment of the model's effectiveness.

Based on the above procedure, the complete fault diagnosis workflow proposed in this study is illustrated in Fig. 2, which provides a clear visualization of the overall signal processing, feature extraction, and classification process.

4. Case studies and analysis

4.1. Dataset description

In petroleum drilling operations, the mud pump functions as the core power unit of the drilling rig circulation system, delivering high-pressure drilling fluid to the wellbore. Its operational status directly affects drilling efficiency and safety. The bearing system, as a key component subjected to complex dynamic loads and strong vibrations, is critical for maintaining stable mud pump performance. Bearing degradation can lead to abnormal vibrations, flow instabilities, and, in severe cases, unexpected equipment shutdowns or drilling accidents. Consequently, effective fault diagnosis of mud pump bearings is of considerable engineering significance to ensure reliable and safe operation.

Acquiring high-quality vibration signals from mud pump bearings in actual field conditions is challenging due to harsh operating environments, strong background noise, and limited sensor deployment. To verify the effectiveness and robustness of the proposed diagnostic method under controlled and repeatable conditions, this study utilizes the publicly available Case Western Reserve University (CWRU) bearing dataset as a benchmark. The CWRU dataset provides high-quality vibration signals corresponding to four bearing conditions – normal state, inner race fault, outer race fault, and rolling element fault – by introducing artificial defects of varying types and severities into motor-end bearings. The dataset includes defect diameters of 0.007 in, 0.014 in, and 0.021 in, and supports multiple sampling frequencies, making it a widely adopted platform

for validating bearing fault diagnosis algorithms.

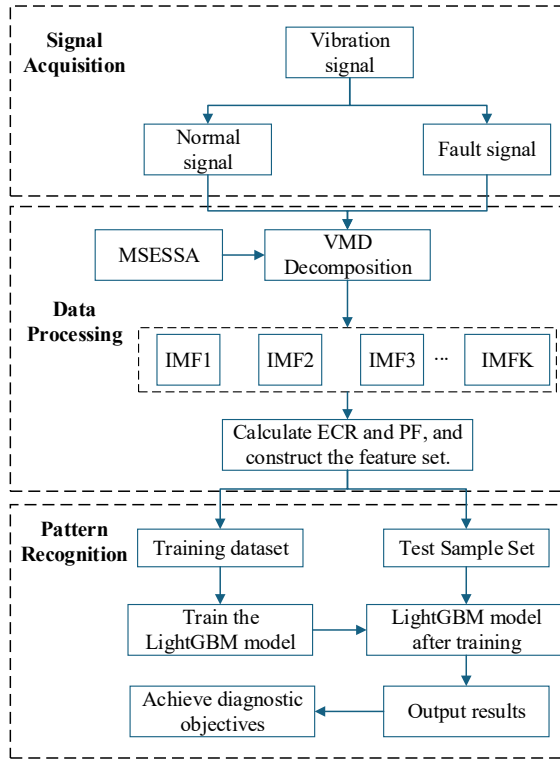

Fig. 2. Fault diagnosis process based on MSESSA-VMD and LightGBM

For this study, vibration signals associated with a defect diameter of 0.007 in were selected, encompassing the normal condition, inner race fault, outer race fault, and rolling element fault. All signals were sampled at 12 kHz, with each segment containing 10,240 data points. Figs. 3-6 display the time-domain waveforms and corresponding frequency spectra for the four typical operating conditions: Fig. 3 shows the normal condition, Fig. 4 the inner race fault, Fig. 5 the rolling element fault, and Fig. 6 the outer race fault.

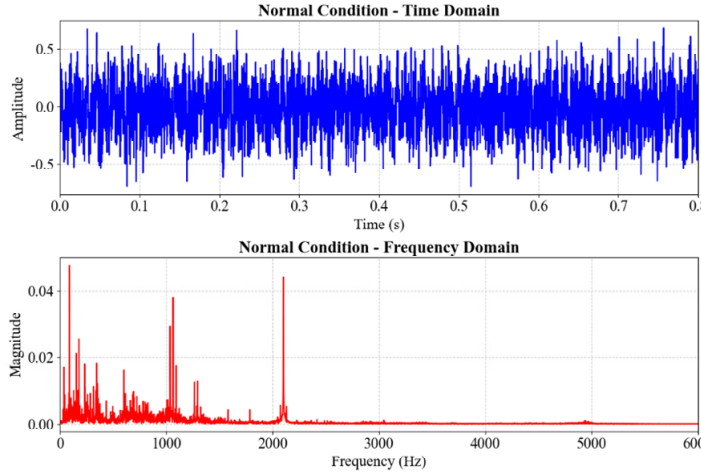

Fig. 3. Time-domain diagram and frequency spectrum diagram of the bearing under normal conditions

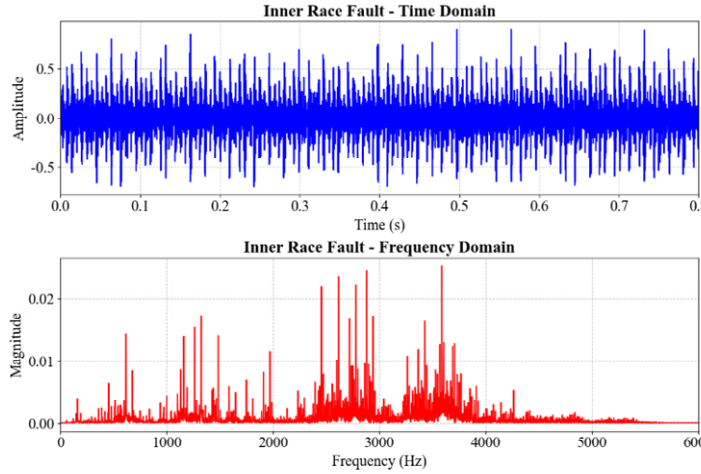

Fig. 4. Time-domain diagram and frequency spectrum diagram of the bearing under inner race fault

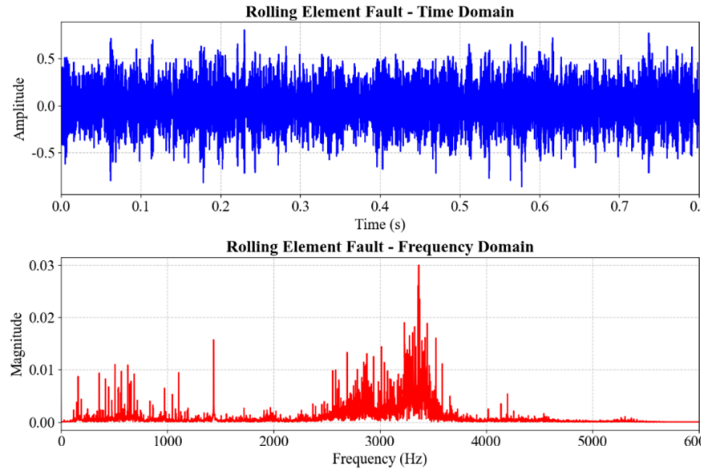

Fig. 5. Time-domain diagram and frequency spectrum diagram of the bearing under rolling element fault

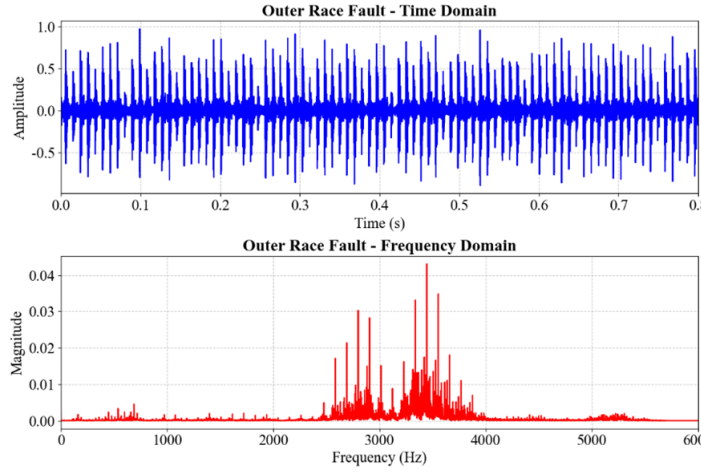

Fig. 6. Time-domain diagram and frequency spectrum diagram of the bearing under outer race fault

ISSN PRINT 1392-8716, ISSN ONLINE 2538-8460

As shown in the figure, under both normal and faulty operating conditions, the vibration signal energy is predominantly concentrated in the low-frequency range (below 1000 Hz) and the mid-to-high-frequency range (2000-5000 Hz). Compared with the normal condition, the faulty states exhibit an overall increase in spectral energy, along with noticeable shifts in the locations and amplitudes of spectral peaks. These observations indicate that bearing faults significantly affect the distribution of energy across multiple frequency bands.

However, the measured vibration signals are often contaminated by noise, particularly in the low-frequency region, which can obscure weak impulsive components associated with early-stage faults. Consequently, differentiating between fault types based solely on conventional time-domain or frequency-domain analysis is challenging. This underscores the importance of employing advanced signal decomposition and feature extraction techniques to enhance fault feature separability and improve diagnostic accuracy.

4.2. Results of VMD parameter optimization using MSESSA

Adaptive optimization of the key VMD parameters – the penalty factor α and the number of decomposition modes K – is performed using the proposed Multi-Strategy Enhanced Sparrow Search Algorithm (MSESSA). The fitness function is formulated as a weighted combination of the mean squared error (MSE) between the original and reconstructed signals and the envelope entropy (EE). While MSE reflects the overall reconstruction fidelity, it may fail to capture subtle fault-related envelope characteristics. In contrast, EE quantifies the instantaneous energy distribution of the signal and is highly sensitive to impulsive components generated by bearing faults. To achieve a balance between accurate reconstruction and preservation of fault-sensitive features, EE is assigned a weight of 0.8, while MSE is weighted at 0.2. This weighting strategy enhances the discriminability of fault-related components and ensures robust decomposition results across varying operating conditions.

In the MSESSA implementation, the population size is set to 20, and the maximum number of iterations is 15. The search range for the mode number K is defined as [2, 12], while the penalty factor α is explored within [200, 8000], covering commonly adopted values in VMD-based fault diagnosis studies and ensuring both optimization effectiveness and algorithmic stability. During each iteration, the multi-strategy mechanisms – including sine-cosine perturbation, Cauchy mutation, and adaptive weight updating – work collaboratively to improve global exploration, prevent premature convergence, and refine the search around promising solutions.

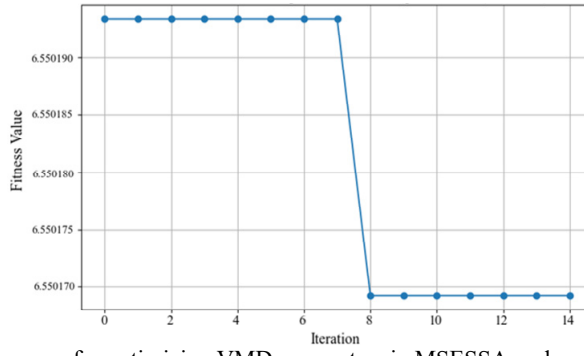

Fig. 7. Iterative curve for optimizing VMD parameters in MSESSA under normal conditions

Figs. 7-10 present the convergence curves of MSESSA under four representative operating conditions: normal state, inner race fault, rolling element fault, and outer race fault. In all cases, the fitness values decrease rapidly within the first 5-6 iterations and gradually stabilize, demonstrating the fast convergence and reliable optimization capability of the proposed algorithm. These results confirm that MSESSA effectively identifies optimal VMD parameters, providing a

solid foundation for subsequent signal decomposition and fault feature extraction. Moreover, the stability of the convergence curves across different fault types highlights the robustness and adaptability of the algorithm for diverse bearing conditions.

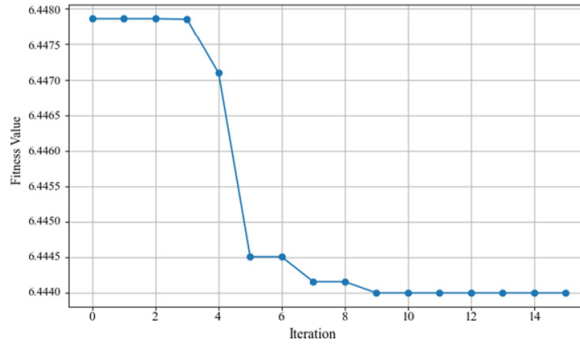

Fig. 8. Iterative curve for optimizing VMD parameters in MSESSA under inner race fault

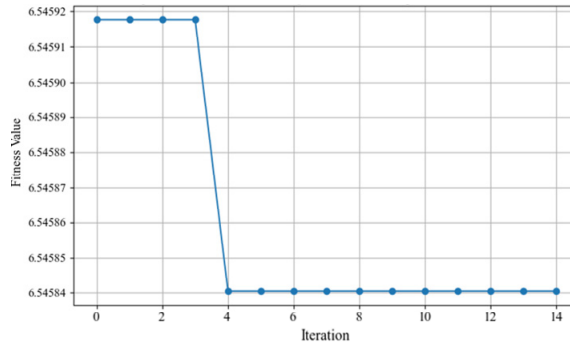

Fig. 9. Iterative curve for optimizing VMD parameters in MSESSA under rolling element fault

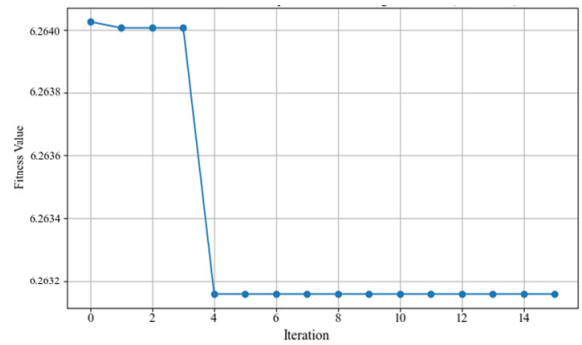

Fig. 10. Iterative curve for optimizing VMD parameters in MSESSA under outer race fault

To further demonstrate the effectiveness of the proposed fitness-driven enhancement scheme, Fig. 10 presents a comparison of the convergence behaviors between the conventional SSA and the proposed MSESSA under the inner race fault condition. In this experiment, both algorithms optimize the same composite fitness function, which jointly integrates Mean Squared Error (MSE) and Envelope Entropy (EE), using a representative inner race fault signal.

The convergence curves show that MSESSA achieves a more rapid reduction in the fitness value and reaches a lower final fitness level compared to the traditional SSA. Because the fitness function simultaneously evaluates signal reconstruction accuracy (via MSE) and modal energy concentration and independence (via EE), a lower fitness value indicates a better balance between

decomposition fidelity and the enhancement of fault-sensitive features.

In comparison with SSA, MSESSA demonstrates superior optimization stability and effectively avoids premature convergence during the early iterations. This improvement is attributed to the multi-strategy enhancement mechanisms embedded in the algorithm. Specifically, the sine–cosine perturbation strategy strengthens global exploration, the Cauchy mutation facilitates escaping local optima, and the adaptive weighting mechanism dynamically balances exploration and exploitation throughout the optimization process. Together, these mechanisms enable MSESSA to more thoroughly navigate the complex fitness landscape defined by the joint MSE–EE objective, achieving more reliable and accurate VMD parameter optimization.

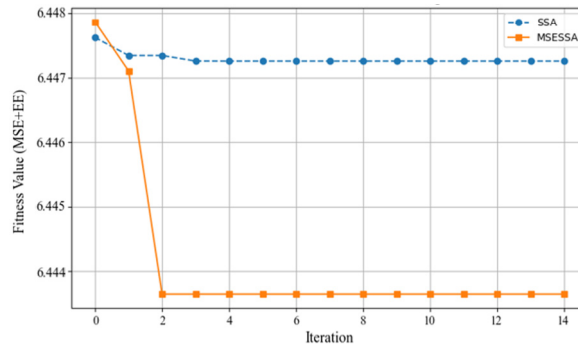

Fig. 11. Convergence comparison between SSA and MSESSA under inner race fault

As shown in Fig. 11, MSESSA converges rapidly within the first few iterations and attains a lower final fitness value (6.4436) compared with SSA (6.4473). Correspondingly, MSESSA identifies a more compact and physically meaningful VMD parameter configuration, with $K = 3$ and $\alpha = 364.56$, whereas SSA converges to a larger number of modes ($K = 6$, $\alpha = 444.22$), potentially introducing redundant or less fault-relevant components.

It should be emphasized that this experiment uses a single representative inner race fault signal to illustrate the convergence behavior of the optimization algorithms under the proposed joint MSE-EE fitness function, rather than to establish statistical robustness. The robustness and generalization capability of the MSESSA-VMD framework are further validated through multi-sample classification experiments presented in later sections.

The optimal VMD parameters for each operating condition are summarized in Table 2.

Table 2. MSESSA-optimized VMD parameter results

Operating condition type	Optimal number of modes K	Optimal Penalty factor α
Normal conditions	4	421.51
Inner race fault	3	400.34
Rolling element fault	10	476.17
Outer race fault	4	211.04

Notably, the mode number K and penalty factor α vary across fault types, reflecting the adaptive nature of MSESSA in handling signals with distinct dynamic characteristics. For instance, $K = 3$ for inner race faults indicates a relatively simple frequency structure, whereas $K = 10$ for rolling element faults corresponds to richer frequency content and stronger non-stationarity. The outer race fault exhibits the smallest penalty factor ($\alpha = 211.04$), allowing VMD to effectively retain low-frequency impact components. Parameters for the normal condition fall between those of the faulty cases, consistent with more uniform and stable vibration characteristics.

Overall, these results demonstrate that MSESSA enhances both global search capability and convergence stability, enabling accurate and adaptive determination of VMD parameters. The

resulting improvements in signal decomposition quality provide a reliable foundation for subsequent IMF selection and multidimensional feature extraction, thereby supporting robust and physically meaningful bearing fault diagnosis.

4.3. MSESSA-VMD decomposition results and spectral analysis

To further assess the signal decomposition capability of the proposed MSESSA-VMD framework, bearing vibration signals under four operating conditions – normal condition, inner race fault, rolling element fault, and outer race fault – are adaptively decomposed using VMD with the optimal parameter sets obtained via MSESSA. Each signal is decomposed into multiple intrinsic mode functions (IMFs), each exhibiting distinct frequency characteristics that reflect the underlying dynamic behavior of the bearing system.

Building on the previous section, where the effectiveness of MSESSA in optimizing VMD parameters was demonstrated, this stage focuses on evaluating how these optimized parameters influence the quality of signal decomposition and the extraction of fault-sensitive components. Specifically, the resulting IMFs are analyzed in both the time and frequency domains to determine their ability to separate fault-related components from background noise and reveal characteristic frequency information unique to each fault type.

Comparative examination of the IMFs across different operating conditions highlights the adaptability and physical meaningfulness of the decomposition achieved by MSESSA-VMD. For instance, under fault conditions, energy tends to concentrate in specific IMFs corresponding to the localized impacts induced by inner race, outer race, or rolling element defects, whereas normal signals exhibit a more evenly distributed modal energy pattern. These observations confirm that MSESSA effectively guides VMD toward stable, adaptive, and physically interpretable modal decomposition, thereby providing a solid foundation for subsequent IMF selection, feature extraction, and accurate fault diagnosis.

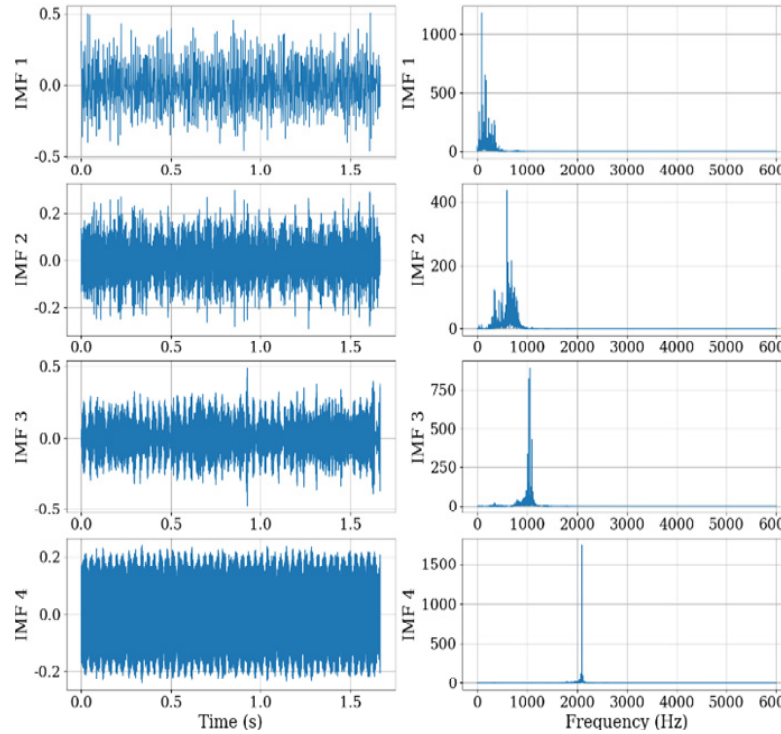

Fig. 12. Time-domain waveforms and spectra of IMFs under normal conditions

ISSN PRINT 1392-8716, ISSN ONLINE 2538-8460

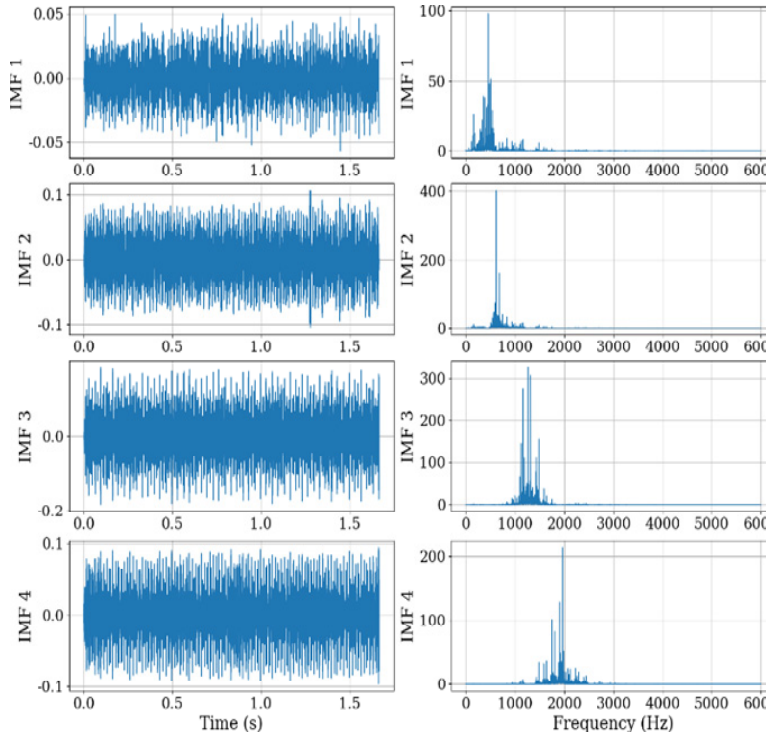

Fig. 13. Time-domain waveforms and spectra of IMFs under inner race fault

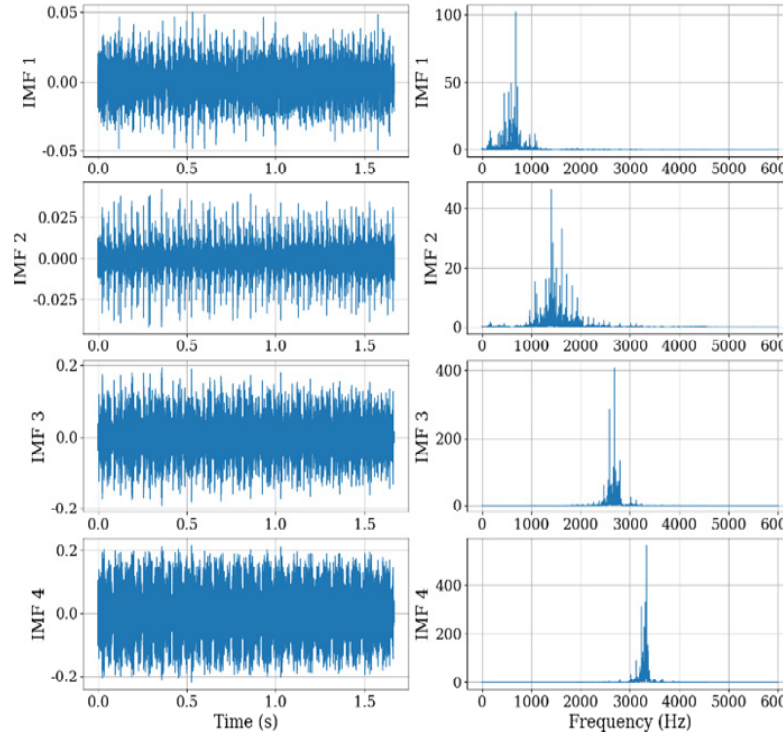

Fig. 14. Time-domain waveforms and spectra of IMFs under rolling element fault

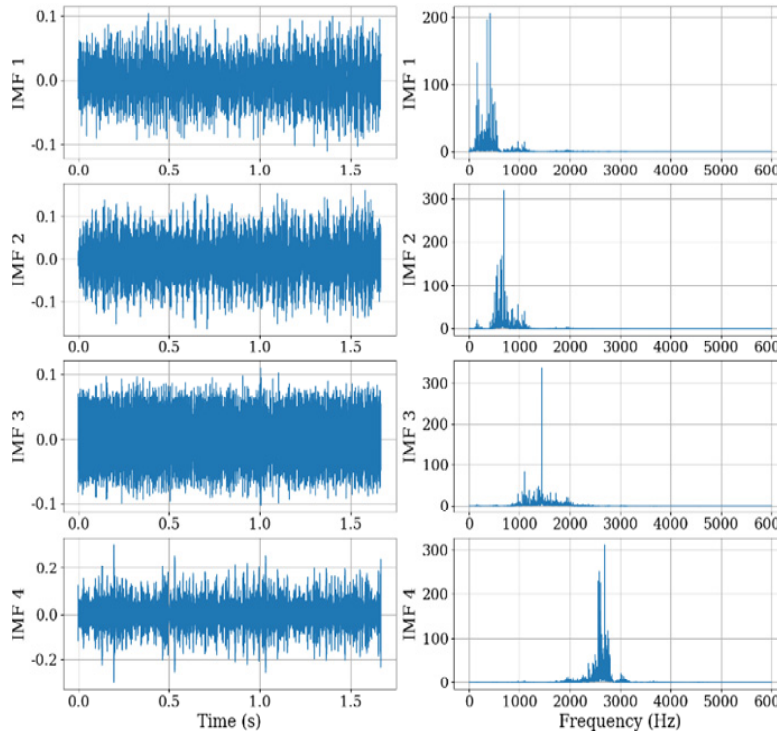

Fig. 15. Time-domain waveforms and spectra of IMFs under outer race fault

From the time-domain perspective, each IMF generated by the MSESSA-VMD method corresponds to vibration components within specific frequency ranges. Low-frequency IMFs predominantly capture the global rotational behavior and load-induced trends of the bearing system, whereas high-frequency IMFs highlight transient impulsive responses associated with localized defects. This hierarchical decomposition facilitates the isolation of fault-sensitive components from low-frequency background fluctuations.

Frequency-domain analysis further indicates that the MSESSA-optimized VMD achieves enhanced frequency clustering, with reduced spectral overlap among adjacent IMFs. Under faulty conditions, the energy of certain IMFs is concentrated within narrow frequency bands, closely matching the theoretical characteristic frequencies of bearing defects, including inner race, rolling element, and outer race faults. This demonstrates that fault-related spectral features are effectively preserved during decomposition.

Compared with conventional VMD using empirically selected parameters, the proposed MSESSA-VMD method offers improved frequency resolution and enhanced modal stability. As a result, more interpretable and reliable time-frequency representations are obtained, providing a solid foundation for subsequent IMF selection, feature extraction, and fault classification.

4.4. IMF filtering and feature extraction results

After MSESSA-VMD decomposition, vibration signals under each operating condition are separated into multiple intrinsic mode functions (IMFs) with distinct frequency characteristics. Due to variations in frequency content and energy distribution, individual IMFs contribute differently to fault feature representation, with some components primarily containing noise or redundant information. Therefore, effective IMF filtering is essential prior to feature extraction to retain fault-sensitive components and suppress irrelevant modes.

In this study, a joint IMF selection strategy based on the Energy Contribution Ratio (ECR) and

Peak Factor (PF) is employed. ECR quantifies the proportion of signal energy carried by each IMF, enabling identification of dominant energy-bearing components, while PF measures signal impulsiveness and is particularly sensitive to localized fault-induced impacts. By considering both indicators simultaneously, IMFs with significant energy contribution and strong impulsive characteristics are effectively preserved.

As illustrated on Fig. 16, prior to IMF filtering, signal energy is distributed across multiple IMFs, including several low-energy components dominated by noise or redundancy. After applying the proposed ECR–PF-based criterion, only a few IMFs with dominant energy contributions and pronounced impulsive behavior are retained.

For the inner race fault condition, IMF3 and IMF4 are identified as the most informative components, collectively accounting for approximately 79 % of the total signal energy and exhibiting higher peak factor values, indicating strong fault-induced impulsive behavior. In contrast, IMF1 and IMF2 contribute less energy and display weaker impulsiveness, suggesting that they mainly capture background vibrations or noise-dominated components.

These findings demonstrate that the proposed IMF filtering strategy effectively suppresses low-information modes while preserving dominant fault-relevant components, providing a reliable and physically meaningful signal basis for subsequent feature extraction and intelligent fault classification.

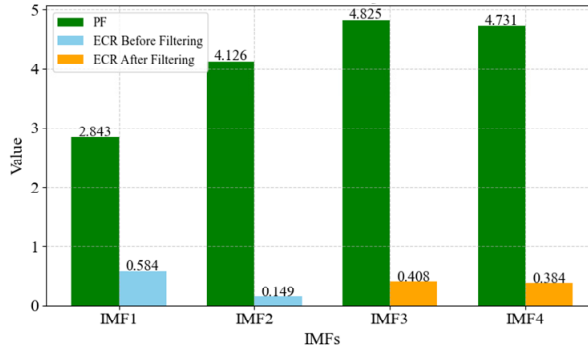

Fig. 16. Comparison of IMF energy contribution and peak factor before and after ECR-PF-based filtering

Figs. 17-20 illustrate the distributions of ECR and PF values for all IMFs under four operating conditions. The results demonstrate that, for different fault types, several IMFs simultaneously exhibit high ECR and elevated PF values, indicating strong fault sensitivity. In contrast, IMFs with low energy contribution and insignificant PF values primarily reflect background noise or low-information content and are therefore excluded from subsequent analysis. The clear differentiation observed in the ECR-PF distributions across operating conditions provides quantitative support for the effectiveness of the proposed joint IMF selection criterion.

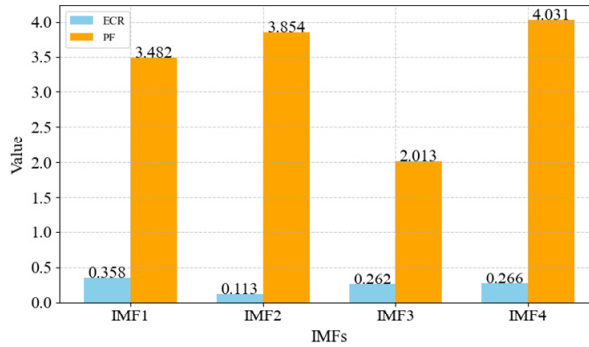

Fig. 17. ECR and PF of each IMF under normal condition

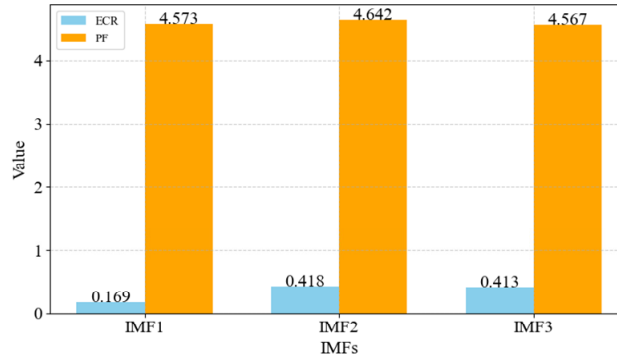

Fig. 18. ECR and PF of each IMF under inner race fault

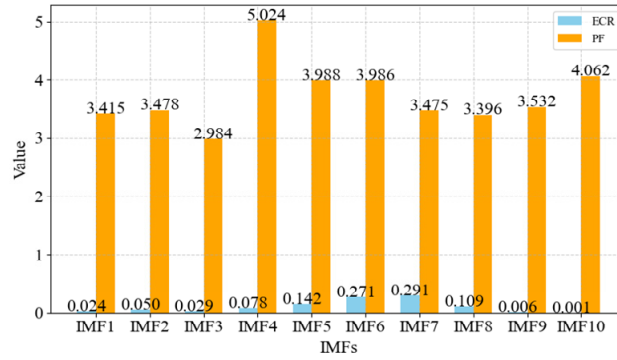

Fig. 19. ECR and PF of each IMF under rolling element fault

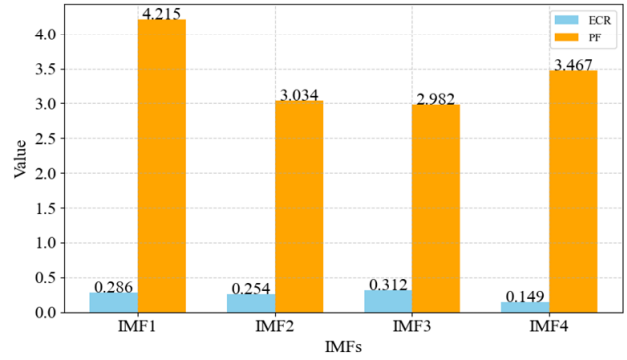

Fig. 20. ECR and PF of each IMF under outer race fault

Under normal operating conditions, the vibration energy is relatively evenly distributed across the intrinsic mode functions (IMFs), with ECR values ranging from 0.113 to 0.358 and PF values between 2.013 and 4.031. This relatively uniform distribution indicates that the vibration signal is mainly governed by stable rotational components and low-amplitude fluctuations. The weak impulsive characteristics reflected by the relatively low PF values suggest that the bearing operates in a stable and healthy state without significant impact events.

For inner race faults, the energy distribution exhibits a clear concentration in IMF2 and IMF3, with ECR values reaching 0.418 and 0.413, respectively. Meanwhile, the PF values increase to approximately 4.5-4.7, indicating pronounced impulsive behavior. This phenomenon corresponds well with the typical vibration characteristics of inner race defects, where localized damage produces periodic impacts each time a rolling element passes over the defect region. As a result,

ISSN PRINT 1392-8716, ISSN ONLINE 2538-8460

a large portion of the fault-related energy is concentrated within the mid-to-high frequency components of the signal.

In the case of rolling element faults, the vibration signal is decomposed into ten IMFs, among which IMF5-IMF7 contain the most significant energy contributions, with ECR values approximately ranging from 0.14 to 0.29. The PF values in this range vary between 3.4 and 4.0. Compared with inner race faults, the energy distribution in this condition is more dispersed across multiple IMFs. This characteristic reflects the complex and highly non-stationary vibration behavior caused by intermittent contact, slippage, and irregular motion of the rolling elements, which introduces richer spectral components and more complex impulsive signatures.

For outer race faults, IMF1-IMF3 dominate the signal energy distribution, with ECR values ranging from 0.254 to 0.312 and PF values between 2.982 and 4.215. Compared with inner race faults, the overall impact intensity is relatively moderate. This indicates that the vibration response is mainly characterized by lower-frequency components and relatively stable periodic impacts. Such characteristics are consistent with localized defects on the outer race located within the load zone, where impacts occur regularly but with comparatively lower intensity.

A comparative analysis across all operating conditions reveals that PF values increase noticeably in fault states, particularly for inner race and rolling element faults, indicating stronger impulsive and non-stationary characteristics in the vibration signals. In contrast, the normal condition exhibits a more uniform energy distribution across IMFs and lower impulsive intensity. The concentrated energy observed in inner race faults suggest localized high-energy impacts, while the distributed energy pattern of rolling element faults reflects greater spectral complexity and dynamic variability.

Based on the joint evaluation criterion combining ECR and PF, a subset of informative IMFs is selected for each operating condition, while noise-dominated or low-information components are discarded. This IMF filtering process effectively enhances the signal-to-noise ratio and preserves the most fault-sensitive components of the vibration signal. From the selected IMFs, discriminative time-domain and frequency-domain features are extracted to capture both statistical and spectral characteristics of the bearing dynamics.

These extracted features are subsequently used as inputs to the LightGBM classifier, which teaches nonlinear relationships between vibration patterns and fault categories. Through this sequential process of adaptive signal decomposition, IMF selection, feature extraction, and intelligent classification, the proposed MSESSA-VMD-LightGBM framework establishes a complete and effective diagnostic pipeline for rolling bearing fault identification under complex operating conditions.

4.5. Fault diagnosis results based on MSESSA-VMD-LightGBM

To evaluate the effectiveness of the proposed MSESSA-VMD framework in feature extraction and its applicability for bearing fault diagnosis, classification experiments were conducted using four representative operating conditions from the CWRU dataset: normal condition, inner race fault, outer race fault, and rolling element fault. The sample sizes for each class were 595 (normal), 885 (inner race fault), 885 (outer race fault), and 900 (rolling element fault). For each condition, 80 % of the samples were randomly selected for training, with the remaining 20 % reserved for testing.

As shown in Fig. 21, the MSESSA-VMD-LightGBM framework achieved an overall classification accuracy of 99.57 % on the test set. Specifically, normal condition, inner race fault, and outer race fault were classified with 100 % accuracy, while rolling element fault achieved 98.3 % accuracy, with only three samples misclassified as inner race faults.

The minor misclassification is attributable to the similarity in impulsive vibration characteristics and partial overlap in frequency components between rolling element and inner race faults under certain operating conditions. Overall, the results indicate that features extracted via MSESSA-VMD exhibit strong discriminative capability, enabling LightGBM to achieve

highly accurate and stable fault identification across all bearing conditions.

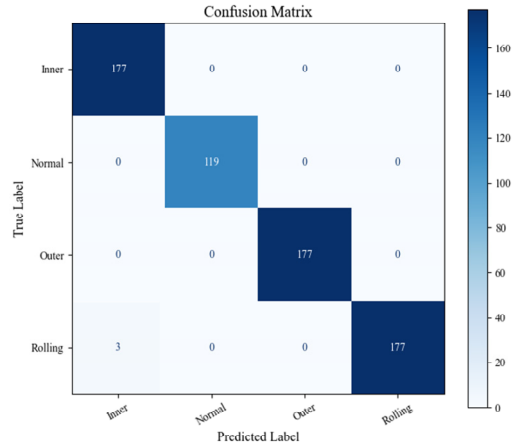

Fig. 21. Confusion matrix of CWRU bearing faults using MSESSA-VMD-LightGBM

Moreover, the results demonstrate that, despite class imbalance and potential noise interference, the features extracted via the MSESSA-VMD framework remain robust and informative, yielding consistent classification performance. This underscores the framework's strong resilience to practical challenges such as uneven sample distributions and signal contamination.

It should be noted that the primary objective of this study is not to develop a novel classifier, but to enhance adaptive vibration signal decomposition and optimize the extraction of fault-relevant features. Accordingly, the classification outcomes serve primarily as a validation tool to assess the effectiveness and practical applicability of the proposed MSESSA-VMD framework, providing an indirect yet meaningful evaluation of its feature representation capability.

4.6. Comparative analysis of method performance

To further assess the effectiveness and generalization capability of the proposed MSESSA-VMD-LightGBM framework, comparative experiments were conducted using various combinations of signal decomposition strategies and classifiers. The main goal of these experiments is to evaluate the impact of VMD parameter optimization under the same composite fitness function and to examine the influence of classifier choice on diagnostic performance, rather than to pursue classifier complexity.

Specifically, five representative diagnostic models were constructed for comparison. The baseline VMD-LightGBM model uses fixed VMD parameters without optimization, providing a reference to assessing the necessity of adaptive tuning. The SSA-VMD-LightGBM model employs the conventional Sparrow Search Algorithm to optimize VMD parameters using the joint MSE-EE fitness function, highlighting the effect of optimization capability on decomposition quality. Additionally, two deep learning–based models, MSESSA-VMD-CNN and MSESSA-VMD-ResNet, were included to compare the proposed lightweight framework against representative convolutional architectures under identical feature extraction conditions. The classification results for all methods are summarized in Table 3.

As summarized in Table 3, the baseline VMD–LightGBM model achieves an overall classification accuracy of 94.12 %, with precision, recall, and F1-score of 93.84 %, 93.55 %, and 93.70 %, respectively. These results indicate that while the model can capture general fault characteristics, some subtle features remain unresolved due to suboptimal decomposition and

noise interference. When conventional SSA is applied for VMD parameter optimization under the joint MSE-EE fitness function, performance improves moderately, with accuracy increasing to 95.48 %, and precision, recall, and F1-score reaching 95.12 %, 94.95 %, and 95.04 %, respectively. This demonstrates that fitness-driven parameter tuning enhances decomposition quality by better balancing reconstruction fidelity and modal energy distribution. However, the modest gain also highlights the limitations of standard SSA in exploring the complex, high-dimensional search space, often resulting in insufficient separation of closely spaced modes or residual noise components.

Table 3. Comparative fault diagnosis performance of different decomposition and classification methods on the CWRU bearing dataset

Model name	Parameter optimization strategy	Accuracy (%)	Precision (%)	Recall (%)	F1-score (%)
VMD-LightGBM	No optimization	94.12	93.84	93.55	93.70
SSA-VMD-LightGBM	Standard SSA	95.48	95.12	94.95	95.04
MSESSA-VMD-CNN	MSESSA	96.72	96.53	96.35	96.44
MSESSA-VMD-ResNet	MSESSA	97.05	96.91	96.82	96.86
MSESSA-VMD-LightGBM	MSESSA	99.57	99.52	99.41	99.46

In contrast, the MSESSA-optimized models consistently outperform both baseline and conventional SSA approaches. The proposed MSESSA-VMD-LightGBM framework achieves the highest overall performance, with an accuracy of 99.57 %, precision of 99.52 %, recall of 99.41 %, and F1-score of 99.46 %. This substantial improvement can be attributed to the multi-strategy enhancements in MSESSA, which simultaneously strengthen global exploration, prevent premature convergence, and adaptively refine VMD parameters. Consequently, modal decomposition is more stable, mode mixing is significantly reduced, and the extracted IMFs contain clearer, more discriminative fault features. The improved feature quality directly translates to enhanced classifier performance, enabling near-perfect identification of bearing fault types across multiple operating conditions.

The deep learning variants, including MSESSA-VMD-CNN and MSESSA-VMD-ResNet, also benefit from optimized decomposition, achieving accuracies of 96.72 % and 97.05 %, respectively. While these models capture hierarchical nonlinear patterns in the features, their marginal advantage over the MSESSA-VMD-LightGBM model suggests that once the IMFs are effectively selected and statistical features are well-extracted, additional complex feature learning contributes little to overall performance. Furthermore, LightGBM offers advantages of lower computational complexity, faster training convergence, and greater interpretability, making it more suitable for practical implementation in industrial fault diagnosis.

Beyond diagnostic accuracy under ideal conditions, it is equally important to evaluate the robustness of the proposed framework when subjected to external interference. To further assess robustness under noisy operating conditions, additive Gaussian noise with SNR levels of 20, 15, 10, and 5 dB was introduced into the vibration signals. The corresponding diagnostic accuracies are summarized in Table 4.

Table 4. Fault diagnosis performance of the proposed MSESSA-VMD-LightGBM framework under different SNR conditions

SNR (dB)	Overall accuracy (%)	Degradation (%)
20	99.08	0.49
15	98.46	1.11
10	97.21	2.36
5	95.63	3.94

As shown in Table 4, the overall classification accuracy gradually decreases as the noise intensity increases, which is consistent with the expected degradation caused by external

interference. Nevertheless, even at SNR = 5 dB, the proposed framework maintains an accuracy above 95 %, demonstrating notable robustness under severe noise contamination.

This behavior can be attributed to the synergistic design of the proposed framework. The VMD algorithm distributes broadband noise across multiple intrinsic mode functions rather than concentrating it within fault-sensitive frequency bands, while MSESSA-based parameter optimization enhances modal independence and suppresses mode mixing. In addition, statistical features such as energy ratio and kurtosis are less sensitive to zero-mean Gaussian noise when computed over sufficiently long signal segments. Combined with the ensemble-based decision mechanism of LightGBM, which tolerates moderate feature perturbations, these characteristics jointly ensure stable classification boundaries even under low SNR conditions.

Overall, the results in Tables 2 and 3 jointly demonstrate that the proposed joint MSE-EE fitness strategy and multi-strategy MSESSA optimization not only enhance modal decomposition quality but also improve fault feature separability and noise robustness. On this foundation, the MSESSA-VMD-LightGBM framework achieves a balanced integration of diagnostic accuracy, computational efficiency, interpretability, and environmental adaptability, highlighting its strong potential for reliable industrial bearing fault diagnosis.

5. Simulation-based fault diagnosis of mud pump bearings

5.1. Simulation signal generation

The effectiveness of the proposed MSESSA-VMD-LightGBM framework was initially validated using the widely adopted CWRU bearing dataset, demonstrating its capability to extract fault-related features and achieve robust classification performance under controlled laboratory conditions. However, to further evaluate the practical applicability of the proposed framework in real mud pump bearing systems, additional validation under more realistic operating environments is necessary.

In oil drilling rigs, acquiring high-quality vibration data from mud pump bearings is extremely challenging due to factors such as variable rotational speeds, fluctuating loads, harsh environmental conditions, and the practical difficulty of conducting controlled fault injections and long-term monitoring. These constraints significantly limit the availability of reliable real-world fault datasets for comprehensive experimental validation.

To overcome these limitations, a simulation-based approach was adopted to generate representative vibration signals for mud pump bearings. The simulation framework was carefully designed to emulate key operational characteristics observed in practical applications, ensuring that the generated signals capture both fault-specific dynamic responses and environmental variability. In general, the simulated vibration signal can be modeled as a superposition of fault excitation, structural response, and noise components, expressed as:

$$x(t) = x_f(t) + x_r(t) + n(t), \tag{15}$$

where $x_f(t)$ denotes the fault-induced excitation, $x_r(t)$ represents the resonance response of the bearing-structure system, and $n(t)$ accounts for background noise and environmental interference.

The simulated signals were generated using the following mechanisms:

(1) Baseline signal parameters.

Each vibration signal was sampled at 12 kHz with a duration of 2 s, consistent with the configuration used in the CWRU dataset. The rotational speed of the mud pump bearing was set to 600 rpm. Based on this speed, the characteristic fault frequencies for inner race, outer race, and rolling element defects were calculated according to standard bearing kinematics theory.

(2) Speed fluctuation and load modulation.

To emulate realistic operating conditions, mild rotational speed fluctuations and periodic load variations were introduced into the simulation model. These factors replicate torque pulsations

and fluid-induced load changes commonly observed during mud pump operation, producing non-stationary amplitudes and frequency modulations in the vibration signals.

(3) Fault-induced impulse generation.

Localized bearing defects – including inner race, outer race, and rolling element faults – were modeled as periodic impulsive excitations at their respective characteristic fault frequencies. To enhance realism, the impulse sequences were modulated by the speed fluctuation model, allowing the simulated signals to capture practical fault-induced vibration behavior under variable operating conditions.

(4) Structural resonance response.

The generated fault impulses were convolved with multiple structural resonance responses to simulate the dynamic interactions between the bearing and its supporting structure. This process reproduces the excitation of resonance modes typically observed in rotating machinery, introducing realistic oscillatory decay characteristics into the simulated signals.

(5) Noise incorporation.

To account for environmental and operational interference, both low-frequency colored noise – representing hydraulic and mechanical background vibrations – and high-frequency Gaussian white noise were added. This hybrid noise model ensures that the simulated data exhibits stochastic characteristics comparable to those encountered in real industrial environments.

(6) Dataset construction.

Based on the above simulation framework, datasets corresponding to four bearing conditions – normal, inner race fault, outer race fault, and rolling element fault – were generated. For each condition, 30 samples were used for training and 10 samples for testing. Although the dataset size is relatively small, the controlled simulation environment allows for a focused evaluation of the proposed MSESSA-VMD feature extraction and LightGBM classification framework under representative mud pump operating conditions. All signals were normalized and stored in MATLAB .mat format to maintain consistency with the CWRU dataset structure, facilitating seamless integration into the subsequent processing pipeline.

By employing this simulation-based strategy, a controlled yet physically meaningful dataset was constructed, enabling systematic evaluation of the proposed fault diagnosis methodology in a mud pump scenario, even in the absence of real field measurements. Fig. 22 presents representative waveforms for each simulated fault type, highlighting the impulsive characteristics of the fault signals and the modulation effects introduced by speed and load variations.

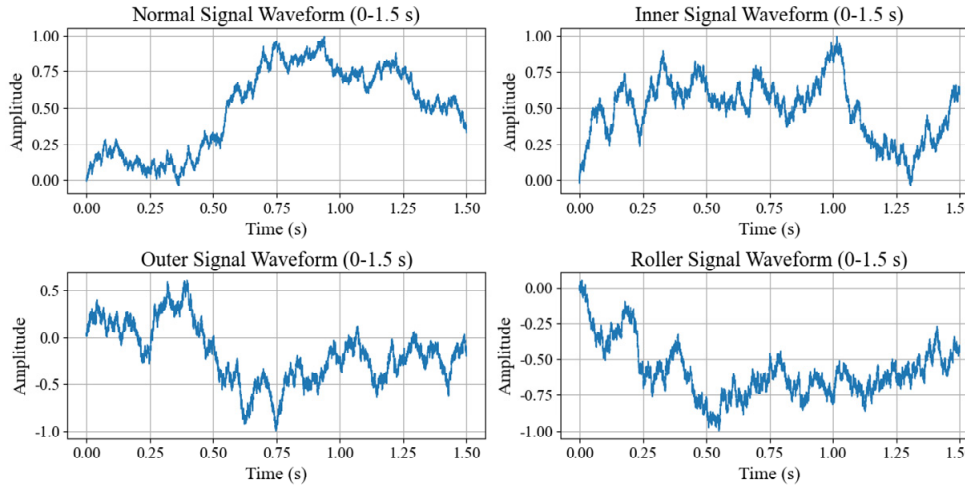

Fig. 22. Time-domain waveforms of simulated mud pump bearing signals under different fault conditions

5.2. VMD parameter selection using MSESSA

To ensure consistency in feature extraction and to enable a fair comparison with the CWRU dataset experiments, the VMD parameters used for decomposing the simulated mud pump bearing signals were directly adopted from the optimal results obtained in the CWRU-based analysis. Specifically, the number of decomposition modes K and the quadratic penalty factor α corresponding to each bearing condition are summarized in Table 5.

Table 5. VMD parameter settings for simulated mud pump bearing signals based on CWRU-optimized results

Operating condition type	Optimal number of modes K	Optimal penalty factor α
Normal conditions	4	450.23
Inner race fault	4	432.67
Rolling element fault	10	520.36
Outer race fault	5	250.05

These parameter configurations were previously optimized using the proposed MSESSA strategy by jointly considering reconstruction accuracy and modal independence. They were shown to produce stable and physically interpretable VMD decompositions across different fault types in the benchmark CWRU dataset. In the present study, the same parameter settings are intentionally reused for the simulated mud pump bearing signals, without any additional parameter tuning, in order to evaluate the robustness and cross-domain transferability of the proposed MSESSA-VMD framework.

From a physical standpoint, the VMD parameters applied to the simulated signals are close to those optimized for the CWRU dataset. This consistency can be attributed to the fact that both datasets represent rolling bearing vibration responses governed by similar underlying physical mechanisms, including periodic fault-induced impacts, structural resonance excitation, and broadband noise interference. Furthermore, the simulated signals were generated using the same sampling frequency and comparable frequency-band characteristics as the CWRU data. Therefore, the similarity in optimized parameter ranges suggests that the selected VMD settings capture intrinsic signal properties rather than dataset-specific artifacts.

Experimental observations further indicate that, under the adopted parameter configurations, the simulated mud pump bearing signals can be effectively decomposed into intrinsic mode functions (IMFs) exhibiting clear frequency separation and minimal mode mixing. Fault-related impulsive components and modulation patterns remain well preserved in the relevant IMFs, thereby providing a reliable basis for subsequent feature extraction and classification. These findings demonstrate that VMD parameters optimized via MSESSA on the benchmark dataset possess satisfactory generalization capability and can be directly extended to simulated mud pump bearing signals, thus supporting the practical applicability of the proposed diagnostic framework.

5.3. Results and discussion

The proposed MSESSA-VMD-LightGBM framework was further evaluated using simulated vibration signals of mud pump bearings under four representative operating conditions, namely normal state, inner race fault, outer race fault, and rolling element fault. The diagnostic performance was assessed based on the classification results obtained from the test samples, and the corresponding confusion matrix is shown in Fig. 23.

The results indicate that the proposed framework achieves an overall diagnostic accuracy of 96.14 % on the simulated dataset, demonstrating its capability to distinguish different bearing fault types under complex noise and modulation conditions. In particular, inner race faults and rolling element faults are identified with high reliability, suggesting that the impulsive and modulation-related vibration features induced by localized defects are effectively captured through the MSESSA-VMD-based signal decomposition and feature extraction process.

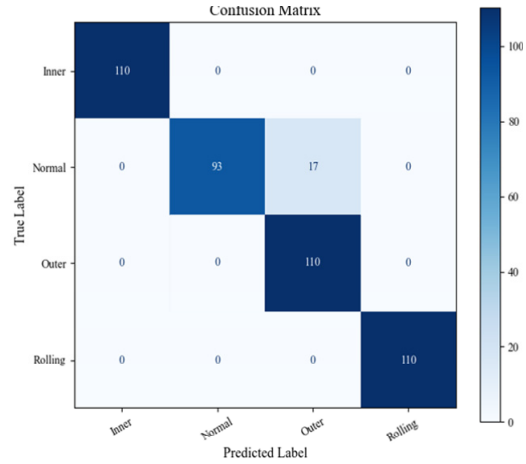

Fig. 23. Confusion matrix of mud pump bearing faults using MSESSA-VMD-LightGBM

A small number of normal-condition samples are misclassified as outer race faults, whereas no fault samples are incorrectly identified as normal. This classification pattern reflects a conservative diagnostic tendency, which is generally desirable in practical condition monitoring applications, as it reduces the risk of missed fault detection (false negatives).

Such misclassification behavior is consistent with engineering experience in bearing fault diagnosis under complex operating environments. Compared with inner race and rolling element defects, outer race faults often produce relatively weaker vibration responses due to longer transmission paths and increased structural damping. Under low-load or variable-load conditions, the vibration characteristics of early-stage outer race faults may partially overlap with those of normal operation, thereby increasing the difficulty of precise discrimination.

Moreover, mud pump systems are inherently subjected to strong hydraulic pulsations, reciprocating excitations, and valve-related impacts, which introduce quasi-periodic components and broadband background noise even during normal operation. These background excitations may resemble low-amplitude fault-induced modulations, leading to conservative misclassification of a limited number of normal samples.

From an industrial perspective, this behavior is acceptable and does not compromise diagnostic reliability, as all fault samples are correctly identified and no false-negative cases are observed. The absence of fault-to-normal misclassification further highlights the safety-oriented characteristics of the proposed diagnostic framework.

Compared with the results obtained using the CWRU bearing dataset, the diagnostic accuracy on the simulated dataset is slightly lower. This outcome is expected given the increased complexity and uncertainty intentionally incorporated into the simulation model, including speed fluctuations, load modulation, structural resonance, and colored noise interference. Despite these challenges, the proposed framework maintains strong feature discriminability and stable classification performance.

Overall, the simulation-based evaluation confirms that the proposed MSESSA-VMD-LightGBM framework is not only effective on standard benchmark datasets but also adaptable to more complex industrial bearing fault diagnosis scenarios. Even in the absence of large-scale field measurements, the proposed approach demonstrates robust diagnostic capability, highlighting its potential applicability to mud pump bearing condition monitoring in realistic engineering environments.

5.4. Ablation study on IMF selection strategy

To further investigate the necessity of the proposed IMF selection mechanism, an ablation

study was conducted by comparing two configurations: (1) feature extraction using all decomposed IMFs without selection, and (2) feature extraction using only the top three IMFs ranked by energy contribution ratio.

Fig. 24 illustrates the confusion matrix obtained when all decomposed IMFs are directly used for feature construction. Under this configuration, the overall diagnostic accuracy reaches 95.23 %.

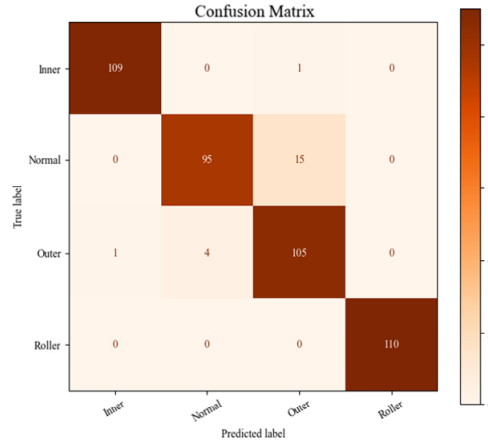

Fig. 24. Confusion matrix of mud pump bearing faults before IMF selection using MSESSA-VMD-LightGBM

Normal condition samples are classified with high reliability, with only one instance misidentified as an outer race fault. Rolling element faults achieve perfect recognition performance. However, noticeable confusion is observed between inner race and outer race faults. Specifically, 15 inner race samples are misclassified as outer race faults, while 4 outer race samples are incorrectly identified as inner race faults.

This bidirectional misclassification suggests partial feature overlap between these two structurally similar fault categories. When all IMFs are retained, low-energy or weakly informative components may introduce redundant statistical features, thereby reducing inter-class separability. Since both inner and outer race defects generate impulsive vibration responses within partially overlapping frequency bands, the presence of redundant IMFs may obscure subtle discriminative characteristics.

Although the overall performance remains high, the observed confusion indicates that further feature refinement may enhance classification robustness.

Fig. 23 presents the confusion matrix obtained after applying the proposed IMF selection strategy. By retaining only the top three IMFs with the highest energy contribution, the overall diagnostic accuracy increases to 96.14 %, representing an improvement of 0.91 % compared with the full-IMF configuration.

Compared with the results without IMF selection, the confusion between inner race and outer race faults is reduced. The number of misclassified samples decreases, indicating improved discriminative capability. By eliminating low-energy IMFs that are more likely dominated by noise or irrelevant background components, the constructed feature space becomes more compact and informative.

In addition to improving classification accuracy, IMF selection reduces feature dimensionality, which may contribute to enhanced computational efficiency and model stability. The improvement, although moderate in magnitude, demonstrates that selective feature construction effectively enhances the signal-to-noise ratio of the extracted fault characteristics.

Fig. 25 provides a direct comparison of classification accuracy between the two configurations. The results clearly indicate that incorporating the IMF selection mechanism improves diagnostic

performance under complex simulated operating conditions.

This ablation study confirms that IMF selection plays a positive role in suppressing redundant signal components and enhancing inter-class separability. Therefore, the selected-IMF configuration is adopted in the final MSESSA-VMD-LightGBM framework.

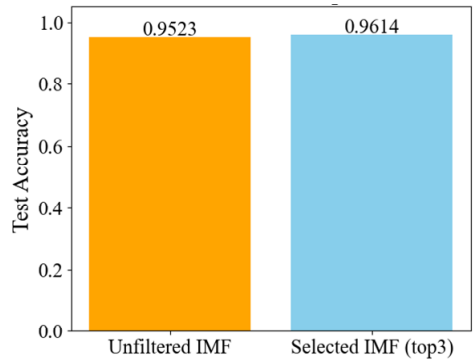

Fig. 25. Comparison of test accuracy between unselected IMFs and top 3 selected IMFs

6. Conclusions

This study proposes an intelligent and adaptive rolling bearing fault diagnosis framework by integrating a multi-strategy enhanced Sparrow Search Algorithm (MSESSA)-optimized Variational Mode Decomposition (VMD) with a Light Gradient Boosting Machine (LightGBM) classifier. The framework is designed to effectively handle the nonlinear, non-stationary, and noise-contaminated characteristics of bearing vibration signals in complex industrial environments.

Experimental validation on the Case Western Reserve University (CWRU) benchmark dataset and simulated mud pump vibration signals demonstrates the effectiveness of the proposed approach. The MSESSA-VMD-LightGBM model achieves a peak classification accuracy of 99.67 % on the benchmark dataset and an average diagnostic accuracy of 96.14 % under simulated industrial conditions, indicating strong robustness against noise interference and signal non-stationarity.

The main contributions of this paper are as follows:

1) Adaptive and physically meaningful feature extraction.

The proposed MSESSA-VMD framework enables automatic optimization of decomposition parameters, producing intrinsic mode functions with enhanced modal independence and fault-related energy concentration. By combining statistical indicators such as energy contribution ratio, envelope entropy, and peak factor, discriminative and noise-resilient features are constructed, improving fault identification reliability.

2) Effectiveness of the dual-objective optimization mechanism.

The proposed fitness function integrates mean squared error (MSE) and envelope entropy (EE) with a weight ratio of 0.2:0.8, balancing signal reconstruction fidelity and fault information concentration. Coupled with the multi-strategy search capability of MSESSA, this optimization demonstrates improved convergence stability and enhanced global exploration compared with conventional SSA, reducing the risk of premature convergence and improving decomposition quality.

3) Balanced performance in accuracy, efficiency, and interpretability.

Compared with deep learning models such as CNN and ResNet, the LightGBM-based framework achieves comparable or superior diagnostic accuracy while maintaining lower computational complexity and better interpretability, making it more suitable for practical industrial deployment with limited computational resources.

4) Engineering applicability under complex operating conditions.

The vibration characteristics in the simulated dataset closely resemble those observed in industrial mud pump bearing systems under strong noise and load fluctuations. Experimental results indicate that the framework can reliably support vibration-based condition monitoring and fault diagnosis in realistic operational scenarios.

Despite the promising performance, several limitations should be acknowledged. The multi-strategy optimization mechanism introduces additional computational cost compared with conventional heuristic algorithms, which may limit its direct application in strict real-time scenarios. In addition, the search boundaries of VMD parameters still require prior specification, which may influence optimization efficiency under highly variable operating conditions. Furthermore, large-scale validation using real industrial mud pump vibration data is necessary to further assess the practical applicability of the proposed method.

Future research will focus on several aspects. First, the proposed framework will be validated using additional industrial datasets and under diverse operating conditions to further evaluate its generalization capability. Second, the integration of deep learning models with the MSESSA-VMD framework will be explored to enhance feature representation and diagnostic performance. Finally, lightweight optimization strategies or parallel implementations will be investigated to improve computational efficiency and support real-time fault diagnosis in practical industrial applications.

Overall, the proposed MSESSA-VMD-LightGBM framework provides a robust, adaptive, and interpretable solution for rolling bearing fault diagnosis under complex operating conditions, offering both methodological contributions and practical potential for industrial condition monitoring.

Acknowledgements

This research was supported by the State Key Laboratory of Large Electric Drive Systems and Equipment Support Technology at Tianshui Electric Transmission Research Institute Group Co., Ltd. The authors also acknowledge Case Western Reserve University for sharing fault data online.

Data availability

The datasets generated during and/or analyzed during the current study are available from the corresponding author on reasonable request.

Author contributions

Chao Zhang: investigation, methodology, writing-original draft. Bing Wang: investigation, methodology, writing-review and editing. Zhenzhong Zhang: supervision. All authors have read and agreed to the published version of the manuscript.

Conflict of interest

The authors declare that they have no conflict of interest.

References

[1] S. Peng, J. Xing, and X. Liu, "A rolling bearing vibration signal noise reduction processing algorithm using the fusion sensors on HPO-VMD and improved wavelet threshold," *Symmetry*, Vol. 17, No. 8, p. 1316, Jan. 2025, https://doi.org/10.3390/sym17081316

[2] M. Kavianpour, P. Kavianpour, A. Ramezani, and M. T. Beheshti, "A partial-imbalance robust domain adaptation framework for bearing fault diagnosis using physics-informed deep learning," *Measurement*, Vol. 257, p. 118890, Jan. 2026, https://doi.org/10.1016/j.measurement.2025.118890

[3] N. E. Huang et al., "The empirical mode decomposition and the Hilbert spectrum for nonlinear and non-stationary time series analysis," *Proceedings of the Royal Society of London. Series A: Mathematical, Physical and Engineering Sciences*, Vol. 454, No. 1971, pp. 903–995, Jan. 1998, https://doi.org/10.1098/rspa.1998.0193

[4] J. Zhou, M. Xiao, Y. Niu, and G. Ji, "Rolling bearing fault diagnosis based on WGWOA-VMD-SVM," *Sensors*, Vol. 22, No. 16, p. 6281, Aug. 2022, https://doi.org/10.3390/s22166281

[5] R. Shi, B. Wang, Z. Wang, J. Liu, X. Feng, and L. Dong, "Research on fault diagnosis of rolling bearings based on variational mode decomposition improved by the niche genetic algorithm," *Entropy*, Vol. 24, No. 6, p. 825, Jun. 2022, https://doi.org/10.3390/e24060825

[6] K. Dragomiretskiy and D. Zosso, "Variational mode decomposition," *IEEE Transactions on Signal Processing*, Vol. 62, No. 3, pp. 531–544, Feb. 2014, https://doi.org/10.1109/tsp.2013.2288675

[7] H. Cui, Y. Guan, and H. Chen, "Rolling element fault diagnosis based on VMD and sensitivity MCKD," *IEEE Access*, Vol. 9, pp. 120297–120308, Jan. 2021, https://doi.org/10.1109/access.2021.3108972

[8] G. Mao and Y. Sun, "A rolling bearing fault diagnosis method based on the improved sparrow search algorithm optimized VMD and multi-scale convolutional neural networks," *Journal of Electronics and Information Science*, Vol. 10, No. 2, pp. 78–87, Jan. 2025, https://doi.org/10.23977/jeis.2025.100210

[9] Z. Hua, Y. Xiao, and J. Cao, "Misalignment fault prediction of wind turbines based on improved artificial fish swarm algorithm," *Entropy*, Vol. 23, No. 6, p. 692, May 2021, https://doi.org/10.3390/e23060692

[10] J. Gu, Y. Peng, H. Lu, X. Chang, and G. Chen, "A novel fault diagnosis method of rotating machinery via VMD, CWT and improved CNN," *Measurement*, Vol. 200, p. 111635, Aug. 2022, https://doi.org/10.1016/j.measurement.2022.111635

[11] M. Demetgul, K. Yildiz, S. Taskin, I. N. Tansel, and O. Yazicioglu, "Fault diagnosis on material handling system using feature selection and data mining techniques," *Measurement*, Vol. 55, pp. 15–24, Sep. 2014, https://doi.org/10.1016/j.measurement.2014.04.037

[12] J. Xue and B. Shen, "A novel swarm intelligence optimization approach: sparrow search algorithm," *Systems Science and Control Engineering*, Vol. 8, No. 1, pp. 22–34, Jan. 2020, https://doi.org/10.1080/21642583.2019.1708830

[13] Y. Xu, W. Cai, L. Wang, and T. Xie, "Intelligent diagnosis of rolling bearing fault based on improved convolutional neural network and LightGBM," *Shock and Vibration*, Vol. 2021, No. 1, pp. 1–13, Jan. 2021, https://doi.org/10.1155/2021/1205473

[14] M. Shao, M. Shi, X. Li, L. Wang, Z. Cai, and D. An, "Cross-domain fault diagnosis of ceramic bearings using multi-source data fusion: vibration, acoustic, and infrared signals," *Proceedings of the Institution of Mechanical Engineers, Part C: Journal of Mechanical Engineering Science*, Vol. 239, No. 21, pp. 8970–8988, Aug. 2025, https://doi.org/10.1177/09544062251355439

[15] Y. Cui, W. Zhang, and Z. Wang, "Abnormal vibration signal detection of EMU motor bearings based on VMD and deep learning," *Sensors*, Vol. 25, No. 18, p. 5733, Sep. 2025, https://doi.org/10.3390/s25185733

[16] F. Han, Y. Zhu, and W. Nie, "Efficient bearing fault diagnosis using depthwise separable convolution and transformer with SSA multi-objective optimization," *International Journal of Pattern Recognition and Artificial Intelligence*, Vol. 39, No. 9, pp. 1–19, May 2025, https://doi.org/10.1142/s0218001425500120

[17] X. Wang et al., "Fault diagnosis method of rolling bearing based on SSA-VMD and RCMDE," *Scientific Reports*, Vol. 14, No. 1, p. 30637, Dec. 2024, https://doi.org/10.1038/s41598-024-81262-9

[18] Y. Mu, Y. Zheng, X. Zhu, H. Guo, L. Wang, and J. Yu, "A bearing fault detection method based on multi-scale attentional feature fusion and Wasserstein generative adversarial network optimization," *Measurement*, Vol. 258, p. 119368, Jan. 2026, https://doi.org/10.1016/j.measurement.2025.119368

[19] X. Wan, F. Liu, A. Wang, F. Liu, M. Zhang, and Z. Pang, "Vibration prediction model of motor bearings for main mine fan based on signal decomposition and improved TCN," *Engineering Research Express*, Vol. 7, No. 3, p. 035413, Sep. 2025, https://doi.org/10.1088/2631-8695/adf598

[20] P. A. Daga et al., "Performance of envelope demodulation for bearing damage detection on CWRU accelerometric data: Kurtogram and traditional indicators vs. targeted a posteriori band indicators," *Applied Sciences*, Vol. 11, No. 14, p. 6262, Jan. 2021, https://doi.org/10.3390/app11146262

[21] B. Yuan, L. Lu, and S. Chen, "Research on bearing fault diagnosis based on vibration signals and deep learning models," *Electronics*, Vol. 14, No. 10, p. 2090, May 2025, https://doi.org/10.3390/electronics14102090

[22] A. Chennana et al., "Vibration signal analysis for rolling bearings faults diagnosis based on deep-shallow features fusion," *Scientific Reports*, Vol. 15, No. 1, p. 9270, Mar. 2025, https://doi.org/10.1038/s41598-025-93133-y

[23] G. Sharma, T. Kaur, S. K. Mangal, N. K. Dhiman, and G. L. Jat, "MEMS approach for rolling bearing fault diagnosis using vibration signal analysis," *Journal of Vibration Engineering and Technologies*, Vol. 13, No. 1, pp. 1–10, Jan. 2025, https://doi.org/10.1007/s42417-024-01730-4

[24] W. Sun, Y. Wang, X. You, D. Zhang, J. Zhang, and X. Zhao, "Optimization of variational mode decomposition-convolutional neural network-bidirectional long short term memory rolling bearing fault diagnosis model based on improved dung beetle optimizer algorithm," *Lubricants*, Vol. 12, No. 7, p. 239, Jan. 2024, https://doi.org/10.3390/lubricants12070239

[25] W. Chen, H. Cai, and Q. Sun, "Bearing fault diagnosis method based on improved VMD and parallel hybrid neural network," *Applied Sciences*, Vol. 15, No. 8, p. 4430, Apr. 2025, https://doi.org/10.3390/app15084430

[26] S. Wang, C. Wang, Y. Lian, and B. Luo, "Research on bearing fault diagnosis based on VMD-RCMWPE feature extraction and WOA-SVM-optimized multidataset fusion," *Sensors*, Vol. 25, No. 16, p. 5139, Jan. 2025, https://doi.org/10.3390/s25165139

[27] A. Yilmaz and M. Aydin, "Determination of Optimal Location of Electrical Vehicle Charging Stations in Istanbul with Genetic Algorithm and Geographical Systems," *International Journal of Informatics Technologies*, Vol. 17, No. 1, pp. 1–9, 2024.

[28] A. K. Mishra, S. K. Sharma, and R. Singh, "Genetic algorithm based approach for optimization of fair power allocation in Pd-NOMA systems," *Tehnicki Vjesnik – Technical Gazette*, Vol. 32, No. 3, pp. 948–957, 2025, https://doi.org/10.17559/tv-20241015002061

[29] Y. Xiao, H. Shao, S. Yan, J. Wang, Y. Peng, and B. Liu, "Domain generalization for rotating machinery fault diagnosis: A survey," *Advanced Engineering Informatics*, Vol. 64, p. 103063, Mar. 2025, https://doi.org/10.1016/j.aei.2024.103063

[30] A. A. Shaalan, W. Mefteh, and A. M. Frihida, "Review on deep learning classifiers for faults diagnosis of rotating industrial machinery," *Service Oriented Computing and Applications*, Vol. 18, No. 4, pp. 361–379, Jul. 2024, https://doi.org/10.1007/s11761-024-00418-7

[31] Y. Lu et al., "Regularity-based evolutionary multi-objective optimization review," *Swarm and Evolutionary Computation*, Vol. 97, p. 101999, Aug. 2025, https://doi.org/10.1016/j.swevo.2025.101999

[32] A. Pătrăușanu, A. Florea, M. Neghină, A. Dicoiu, and R. Chiș, "A systematic review of multi-objective evolutionary algorithms optimization frameworks," *Processes*, Vol. 12, No. 5, p. 869, Apr. 2024, https://doi.org/10.3390/pr12050869

[33] J. L. J. Pereira, G. A. Oliver, M. B. Francisco, S. S. Cunha, and G. F. Gomes, "A review of multi-objective optimization: Methods and algorithms in mechanical engineering problems," *Archives of Computational Methods in Engineering*, Vol. 29, No. 4, pp. 2285–2308, Oct. 2021, https://doi.org/10.1007/s11831-021-09663-x

[34] W. Li and T. Li, "Comparison of deep learning models for predictive maintenance in industrial manufacturing systems using sensor data," *Scientific Reports*, Vol. 15, No. 1, p. 23545, Jul. 2025, https://doi.org/10.1038/s41598-025-08515-z

[35] X. Si, H. Yan, Y. Hu, J. Duan, and T. Shi, "Bearing fault diagnosis under heavy noise: A multi-scale dilated convolution and dense temporal convolutional network," *Neurocomputing*, Vol. 652, p. 131092, Nov. 2025, https://doi.org/10.1016/j.neucom.2025.131092

[36] C. Li, J. Zhou, X. Wu, and T. Liu, "Adaptive feature mode decomposition method for bearing fault diagnosis under strong noise," *Proceedings of the Institution of Mechanical Engineers, Part C: Journal of Mechanical Engineering Science*, Vol. 239, No. 2, pp. 508–519, Oct. 2024, https://doi.org/10.1177/09544062241281840

[37] T. Li, Q. He, and Z. Peng, "Mono-trend mode decomposition for robust feature extraction from vibration signals of rotating machinery," *Mechanical Systems and Signal Processing*, Vol. 200, p. 110583, Oct. 2023, https://doi.org/10.1016/j.ymssp.2023.110583

[38] S. Li, N. Jin, A. Dogani, Y. Yang, M. Zhang, and X. Gu, "Enhancing LightGBM for industrial fault warning: An innovative hybrid algorithm," *Processes*, Vol. 12, No. 1, p. 221, Jan. 2024, https://doi.org/10.3390/pr12010221

[39] D. Bagci Das, "Real-time adaptable fault analysis of rotating machines based on marine predator algorithm optimised LightGBM approach," *Nondestructive Testing and Evaluation*, Vol. 40, No. 3, pp. 831–866, Mar. 2025, https://doi.org/10.1080/10589759.2024.2328750

[40] P. Monteiro, J. Lino, R. E. Araújo, and L. Costa, "Comparison between LightGBM and other ML algorithms in PV fault classification," *EAI Endorsed Transactions on Energy Web*, Vol. 11, No. 1, p. 4865, Jan. 2024, https://doi.org/10.4108/ew.4865

[41] Y. You et al., "Extraction of fault features in rolling bearings via VMD and fuzzy entropy techniques," *Journal of Mechanical Science and Technology*, Vol. 39, No. 10, pp. 5851–5861, Oct. 2025, https://doi.org/10.1007/s12206-025-0921-y

Zhang Chao is a senior engineer who graduated from the Department of Petroleum Engineering at Southwest Petroleum Institute in 1999. He is currently engaged in technical work related to drilling and completion equipment. He is based at the Bohai Petroleum Administration Bureau, No. 2121 Haichuan Road, Binhai New Area, Tianjin, China.

Wang Bing is an intermediate engineer who graduated from Hebei University of Technology in 2010 with a degree in Electrical Automation. He is currently engaged in the design and construction of offshore oil drilling and repair equipment.

Zhenzhong Zhang joined the School of Mechanical Engineering and Rail Transportation and the School of Intelligent Manufacturing Industry at Changzhou University in December 2021. He is a professor and serves as a master's thesis advisor.